Structural relaxation and defect annihilation in pure amorphous silicon

S. Roorda* and W. C. Sinke†
Fundamenteel Onderzoek der Materie (FOM), Institute for Atomic and Molecular Physics, Kruislaan 407, 1098 SJ Amsterdam, The Netherlands

J. M. Poate, D. C. Jacobson, S. Dierker,‡ B. S. Dennis, and D. J. Eaglesham
AT&T Bell Laboratories, Murray Hill, New Jersey 07974

F. Spaepen
Division of Applied Sciences, Harvard University, Cambridge, Massachusetts 02138

P. Fuoss
AT&T Bell Laboratories, Holmdel, New Jersey 07733

(Received 17 October 1990; revised manuscript received 21 March 1991)

Thick amorphous Si layers have been prepared by MeV self-ion-implantation and the thermodynamic and structural properties examined by calorimetry, Raman-spectroscopy, and x-ray-diffraction techniques. Defects have been introduced into well-annealed amorphous and single-crystal Si by He, C, Si, and Ge bombardment. The defect structures are examined by these techniques and by transmission electron microscopy. The structure of amorphous Si in intermediate states of relaxation or annealing have been determined. It is shown that amorphous Si formed by either implantation or deposition contains a large population of point defects and point-defect clusters. Amorphous Si formed by laser quenching cannot be distinguished from well-annealed amorphous Si. Structural relaxation, also known as short-range ordering, can be understood as annihilation of a large fraction of these defects. Both structural relaxation in amorphous Si and defect annihilation in crystalline Si obey bimolecular reaction kinetics. The defect-formation and -annihilation processes are similar in amorphous and crystalline Si. Defect saturation occurs in amorphous Si at estimated defect concentrations of about 1 at. %. These formation and annihilation properties are intrinsic to pure amorphous Si. For hydrogenated amorphous Si, it is pointed out that the metastable-defect-creation and -annealing processes are essentially different from the annihilation processes in pure amorphous Si.

I. INTRODUCTION

The interest in amorphous Si (*a*-Si) lies in two main areas. First, *a*-Si is the model system of an "ideal" covalently bonded continuous random network (CRN).[1–6] Its properties and especially the differences between *a*-Si and crystalline Si (*c*-Si) clearly illustrate the influence of disorder on the physics of solids. Second, in its hydrogenated form *a*-Si (*a*-Si:H) shows semiconducting behavior and can be doped.[7,8] Because *a*-Si:H can be prepared in thin-film form, it can be used in devices, such as solar cells.[9]

One of the most prominent differences between *a*-Si and *c*-Si is that many properties which are well defined in *c*-Si are found to be variable in *a*-Si, and to depend on the thermal history and/or preparation conditions. Examples of such properties are the electron-spin density,[10,11] luminescence,[12] infrared optical properties[13–15] and optical band gap,[16] conductivity,[17,18] vibrational properties,[19–21] enthalpy,[22,23] and atomic structure as probed by electron[24,25] or x-ray[26,27] diffraction and x-ray absorption spectroscopy.[28] Some of these variations are related to macroscopic effects (for example, removal of internal surfaces and voids from sputtered or vacuum-evaporated material[29–31] and some, in the case of *a*-Si:H, to changes in the concentration and bonding of H.[32] However, most are regarded as characteristic of the microscopic structure of a random network.

For *a*-Si prepared by ion implantation, recent measurements of the density have shown it to be $\approx(1.8\pm0.1)\%$ less dense than *c*-Si.[33] Moreover, the density was found to be unchanged within the experimental accuracy after annealing to temperatures up to 580 °C, indicating that changes in vibrational, structural, and thermodynamic properties of ion-implanted *a*-Si are intrinsic to the CRN and are distinctly different from densification involving removal of macroscopic voids sometimes observed in deposited films.[29–31] The transition from the as-prepared to a thermally annealed state is irreversible, and is known as structural relaxation or short-range ordering. In this paper, we will use the term "structural relaxation" exclusively in this sense and not for densification.

Structural relaxation has been viewed as a process to which every atom in the CRN contributes, as is reflected by the observation that the average network parameters, especially the average tetrahedral-bond-angle distortion $\Delta\Theta$, vary continuously as relaxation proceeds.[34] It is also known as short-range ordering.[35] In addition, defects may play an important role in structural relaxation. Since *a*-Si is formed via highly nonequilibrium processes,

 ©1991 The American Physical Society

it is to be expected that the network contains a high concentration of structural defects. In view of the similar structure of *a*- and *c*-Si (both are fourfold coordinated, covalently bonded) the defects in *a*-Si are likely to be similar to the point defects and small point-defect clusters in heavily damaged irradiated *c*-Si. Which role these defects play in structural relaxation is not clear.

In this paper we present a study of the nature of structural relaxation in pure *a*-Si.[36] Differential scanning[22,37] (DSC) and isothermal (DIC) calorimetry,[27] Raman spectroscopy,[38] and x-ray diffraction[39] (XRD) are the main experimental probes, used to characterize *a*-Si which was brought into different intermediate states of relaxation, as well as the kinetics and temperature dependence of the relaxation process. The intermediate states were reached either by thermal treatment of as-prepared *a*-Si, or by the introduction of ion-beam-induced damage in 500 °C relaxed *a*-Si. Most experiments have been performed on *a*-Si prepared by ion implantation. Some additional measurements have been made on vacuum-evaporated and laser-quenched *a*-Si. Pure, rather than hydrogenated *a*-Si has been used, therefore the results are thought to be characteristic of the *a*-Si network and not due to defect passivation by H chemical bonding. Our results strongly indicate that in this material, structural relaxation and point-defect annihilation are intimately related, or rather that relaxation should be primarily regarded as a defect annihilation process.

Most of the experimental details concerning sample preparation and measurement techniques are presented in the following section. The results are presented in Secs. III–VII, and followed by a discussion and conclusions.

II. EXPERIMENTAL PROCEDURES

A. Sample preparation

1. Amorphization by ion implantation

The majority of the implantations was performed at the NEC 1.8-MeV tandem accelerator facility of AT&T Bell Laboratories[40] and others were performed at the 1-MeV HVEE single-ended heavy ion implanter at Fundamenteel Onderzoek der Materie (FOM).[41] "Standard" *a*-Si samples were prepared as follows: Monocrystalline Si targets of either (100) or (111) orientation were implanted with $^{28}Si^+$ ions of 0.5, 1, and 2 MeV. The ion dose at each energy was 5×10^{15} ions/cm^2. The ion beam was defocused to a spot of ≈ 1 cm^2 and scanned electrostatically over a 2×2 or 4×4 cm^2 aperture, behind which the samples were mounted. In order to prevent beam heating effects, the total power on target never exceeded 10 W. In addition, samples were clamped on a copper block which was filled with liquid nitrogen. To ensure a good thermal contact between the sample holder and the Si samples, a thin layer of silicone vacuum grease was used. The sample holder was rotated such that the surface normal of the samples was at an angle of $\approx 7°$ with the ion beam, in order to prevent channeling. These implantations result in the formation of ≈ 2.0-μm-thick *a*-Si layers, as determined by Rutherford backscattering (RBS) in conjunction with channeling of either 3- or 4-MeV He^+ or 1-MeV H^+ ions. To calculate the thickness from the backscatter spectra,[42] stopping powers for He in Si were used as determined by Santry and Werner.[43] In case of the H^+ backscattering measurements, H^+ stopping powers were used which were scaled from D^+ stopping powers in Si.[44]

A familiar problem with ^{28}Si implantations on single-ended accelerators is contamination of the ion beam with $^{14}N_2{}^+$ ions. When a tandem-type accelerator is used, negatively charged ions are extracted from the ion source, accelerated to the terminal voltage, and led through a gas stripper cell. The stripper cell removes one or more electrons from the ion, and the now positively charged ion is further accelerated to earth potential. There are two effects which greatly reduce the N_2 contamination. First, the ionization probability to form negatively charged N_2 is very low, and second, the stripper cell not only removes electrons but also leads to dissociation of molecular ions in the beam.

For implants at the single-ended accelerator at FOM, the contamination of $^{14}N^+$ ions in the beam was determined in two ways. (1) The relative intensity of the 28, 29, and 30 mass beams was compared with the natural abundance of Si isotopes, and (2) the amount of coimplanted N atoms was measured directly by RBS by performing a high-dose implantation in graphite. It was found that the contamination in the beam was less than 5%, which limits the beam-induced concentration of N in the *a*-Si layers to 20 ppm. During these implants, the power on target was kept below 0.25 W, and the samples were again cooled using liquid nitrogen.

For DSC measurements, double-sided polished *c*-Si disks of 7.6-mm diameter and 100-μm thickness were used. Both sides were implanted to a depth of 2.0 μm,[45] yielding ≈ 15 μmol of *a*-Si per disk. Before implantation, the disks were annealed in vacuum ($<10^{-7}$ mbar) for 1 h at 800 °C to remove any possible remnant of crystal damage from dicing or polishing. This ensures that the disks are absolutely thermally stable up to the highest temperature of interest in our DSC measurements.

Thicker layers for XRD measurements were made by additional Si implants at 3.5 and 5 MeV at doses of 6 and 7×10^{15} ions/cm^2, respectively. Rectangular samples of 1×2 cm^2 were used. As a result of the extra implants, the thickness of the *a*-Si layer increased to ≈ 3.6 μm.

2. Evaporation

Deposited *a*-Si films were prepared by *e*-gun evaporation in a vacuum chamber which was pumped by turbomolecular and Ti sublimation pumps. In addition, liquid-nitrogen-cooled shields were used. The system base pressure was $\approx 1\times10^{-8}$ mbar and rose to $\approx 1\times10^{-7}$ mbar during deposition. Before actual deposition the source material was allowed to degas. A small amount of Ti was evaporated before opening the shutter in front of the target; this serves to getter oxygen from the vacuum system. The substrates consisted of 7.6-mm-diameter *c*-Si disks, similar to those used for implanted *a*-Si layers. During deposition at a rate of ≈ 1.5 Å/s, the temperature of the targets was approximately 50 °C.

Before venting the vacuum chamber, the deposited films were first brought to a temperature a 210 °C for a period of 1 h. This densifies the deposited layers,[46] which would otherwise contain interconnected voids leading to substantial indiffusion of oxygen and/or water vapor.[29] The coverage of the deposited layers was measured by RBS of 1.8-MeV He^+ ions and found to be 2.2×10^{18} atoms/cm^2. No oxygen could be detected by RBS measurements which limits the oxygen content to be less than 3 at. %.

3. *Laser quenching*

Laser-quenched *a*-Si samples were prepared by Yater at Cornell University[47] using pulsed laser irradiation of (100) and (111) *c*-Si crystals. The duration of the laser pulse was 3 ns, the wavelength 266 nm, and the pulse energy density ranged from 0.25 to 1 J/cm^2. Hot spots were removed using spatial filtering through a 25-μm-sized pinhole. The lateral intensity distribution of the spatially filtered laser beam is that of a Gaussian. This leads to lateral variations in the thickness of the *a*-Si layer formed. The average thickness amounts to 70 nm on (100) Si and 110 nm on (111) Si substrates, and the typical diameter of a spot thus prepared is $\approx$3 mm. Laser-quenched samples are too small to be used in DSC measurements, and were used for Raman analysis only.

4. *Displacement damage by ion bombardment*

Amorphous silicon which had previously been relaxed by thermal annealing in vacuum at 500 °C for 45 min was subjected to bombardment with a variety of energetic ions. He^+, C^+, Si^+, and Ge^+ ions were used with energies from 50 keV to 8 MeV and fluences from 10^{11} to 10^{16} ions/cm^2. In addition, pieces of *c*-Si were simultaneously subjected to the same bombardments as received by the relaxed *a*-Si samples. During these bombardments the samples were again held at liquid-nitrogen temperature as described above.

Two different mechanisms are responsible for the slowing of fast ions in Si, which are called electronic and nuclear stopping.[48] Electronic stopping is due to interaction of the ion with electrons in the solid (e.g., excitation or ionization of target atoms). Nuclear stopping is the result of violent collisions of the ion with nuclei of target atoms leading to momentum transfer from the ion to the target atom. If the momentum transfer is high enough this may lead to the displacement of the target atom from its lattice position. Electronic and nuclear stopping depend in a different way on the projectile mass and energy.

The number of collision-induced displacements per atom (DPA) in the target material was estimated using Monte Carlo simulations.[48–50] These simulations were performed assuming a threshold displacement energy of 15 eV, a lattice binding energy of 2 eV, and included displacements by recoil Si atoms. The ion damage dose in DPA was calculated by multiplying the ion dose with the number of displaced atoms per incident ion. It is essential here that pure *a*-Si was used in the experiments; in *a*-Si:H two types of displacements damage occur, one being related to Si displacements and one to H displacements. It should be noted that both the threshold energy and cross section for displacement in *a*-Si:H are different for H and Si.

To prepare samples for Raman analysis, high-energy ion irradiation was used to give a uniform damage profile in a 0.1-μm-thick surface layer roughly corresponding to the probe depth of Raman measurements. Ion-beam-damaged *a*-Si for DSC was prepared using multiple energy bombardments, such that all radiation damage was confined in the *a*-Si layer, resulting in a reasonably uniform damage profile. The ion mass–energy–dose combinations leading to 1 DPA in either a 0.1-μm-thick surface layer (for Raman) or a 2-μm-thick surface layer (for DSC) are shown in Table I. The ion damage doses used in the experiments ranged from 0.003 to 1 DPA.

B. Characterization techniques

1. *Differential calorimetry*

Most DSC and DIC measurements were performed at Harvard University using a Perkin Elmer DSC-2 instrument. Earlier measurements[22] were done at Philips Research Laboratories, Eindhoven, employing a Perkin Elmer DSC-7. The DSC-2 instrument was equipped with a new, stable measurement head and a PC for data acquisition. The samples were not in direct contact with the DSC furnace pans, but rested on graphite spacers. During the measurements the sample pans were flushed with pure Ar which had passed through a heat bath stabilized at 25 °C. Unimplanted *c*-Si samples of the same size as the measured samples were loaded in the reference DSC pan in order to balance the thermal load of the instrument.

After loading of the samples but before each measurement, the calorimeter was allowed to equilibrate for several minutes. Scans ran from 50 °C to the end temper-

TABLE I. Post-anneal bombardment conditions (normalized to 1 DPA).

Raman or DSC	Ion species	E_1 (MeV)	Dose 1 (10^{15}/cm^2)	E_2 (MeV)	Dose 2 (10^{15}/cm^2)	E_3 (MeV)	Dose 3 (10^{15}/cm^2)
Raman	C^+	4.5	125				
Raman	Si^+	5.5	16				
Raman	Ge^+	8.3	2.5				
DSC	He^+	0.05	7	0.12	7	0.2	12
DSC	Si^+	0.5	0.5	1.5	1		
DSC	Ge^+	0.7	0.2	2.2	0.4		

ature at 40 K/min; the instrument was held at the end temperature for a few minutes (when DCS measurements were taken) or for a longer period (when DIC measurements were recorded). After cooling down from the first scan, a second scan was taken without touching the samples between scans. Ideally, subtraction of the second curve from the first gives the heat release from the damaged material during the first scan. However, baseline corrections were sometimes necessary as will be shown in Sec. IV. The temperature scale of the DSC instrument was calibrated using the melting point of In and a solid-solid phase transition in K_2CrO_4 and the power scale was calibrated using the specific heat of pure sapphire.

For DIC measurements at 200 °C, 350 °C, and 500 °C, the DSC instrument was loaded with six Si disks, implanted on both sides. This corresponds to an amount of ≈0.1 mmol *a*-Si. For DSC measurements of samples which were brought to an intermediate state of relaxation using thermal annealing, the instrument was loaded with three double-sided implanted disks. For measurements of *c*-Si or relaxed *a*-Si samples which had been subjected to ion-beam-induced damage doses of 0.003–1 DPA, only two disks were used which had been bombarded on one side only. In those cases, the amount of ion-beam-damaged *a*-Si in the instrument amounted to ≈9 μmol.

2. *Raman spectroscopy*

Stokes Raman spectra were recorded using the 488-nm line from an Ar-ion laser. Other Ar plasma lines were removed using a monochromator. The laser was focused to a rectangular spot of ≈50×200 μm and the power on target was kept below 150 mW. The light incident on the samples was horizontally polarized. Raman spectra were recorded using either *HH* or *VH* polarization geometry (*V* is vertical, *H* is horizontal). A triple stage monochromator dispersed the Raman spectrum onto a charge-coupled device (CCD) camera. One spectrum could be recorded with sufficient statistics in a few minutes.

Spectra of *a*-Si were characterized by the position and half-width (at the high-wave-number side) of the TO-like peak. These parameters may be used as an indicator for the state of relaxation of *a*-Si. A peak position at high frequency (≈479 cm^{-1}), and a small peak width (≈35 cm^{-1}) indicate anneal-stable *a*-Si, whereas a lower-frequency peak position (≈471 cm^{-1}) and a broad peak (≈43 cm^{-1}) are indicative of "unrelaxed" or "as-implanted" *a*-Si.[21,22,51]

TABLE II. Parameters describing kinetics of structural relaxation in *a*-Si.

Temperature (°C)	τ_i (dominant) (s)	τ (bimolecular) (s)	E_i (eV)
200	113	74	1.4
350	107	73	1.9
500	115	95	2.3

3. *X-ray diffraction*

X-ray scattering measurements were performed using the AT&T beamline X16C at the National Synchrotron Light Source (Upton, NY). X16C is an unfocused beamline with a double crystal, parallel setting monochromator with Si(111) crystals. For the measurements shown here, it was operated at a photon energy of 11 192 eV and with a 0.5-mm-vertical by 3-mm-horizontal acceptance. The estimated photon flux was 3×10^9 photons/s. The x-ray diffractometer system used the standard arrangement of (1) an incident I_0 monitor consisting of a Kapton film scattering a small fraction of the x rays 90° into a NaI(Tl) detector, (2) a small Huber diffractometer, (3) a 0.4° acceptance Sollar slit to collimate the scattered x rays in the diffraction plane, and (4) a NaI(Tl) detector to measure the scattered x rays. The sample was contained in a small vacuum can with Kapton windows that was periodically pumped with a roughening pump.

Symmetric Bragg scans yielded unacceptably high contributions from the monocrystalline substrate. Therefore, the measurements shown here were obtained with the incident (Θ) angle fixed at 2°. Even in that case, alignment of the crystal along one of the principal [e.g., with the (110) parallel to the incident beam] yielded strong substrate reflections. Thus, the sample for each measurement was carefully rotated 10° about the surface normal away from the (110). This procedure yielded acceptable scattering patterns from the *a*-Si layer with no obvious contamination of bulk scattering.

III. KINETICS OF RELAXATION DETERMINED BY ISOTHERMAL CALORIMETRY

A. Unimolecular and bimolecular reaction kinetics

Figure 1 shows the DSC and the DIC difference traces at 200 °C, 350 °C, and 500 °C of *a*-Si as prepared by ion implantation ("as-implanted"). The heating rate during the DSC part of the measurement was 40 K/min. The dotted vertical lines serve to separate the scanned from the isothermal measurements. The traces to the left of the dotted lines represent the scanned (DSC) trace. A

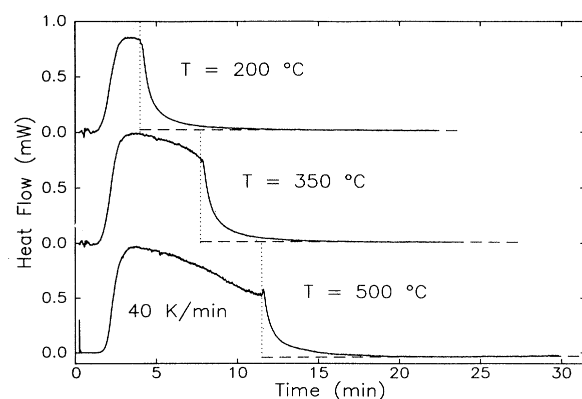

FIG. 1. DSC and DIC difference traces of as-implanted *a*-Si. Dotted lines serve to separate the DSC and DIC signals. Dashed lines are discussed in the text.

positive signal corresponds to a heat release by the *a*-Si during the first run. The time axis for this part of the curve may be converted to a temperature axis using the heating rate and the begin temperature (50 °C) at $t = 0$. The traces to the right of the dotted lines are the isothermal (DIC) measurements at each of the end temperatures (T_{iso}), beginning at the time indicated by the dotted lines.

After 10 min at T_{iso}, all three isotherms have stabilized. Linear least-squares fits have been made to the part of the isotherms, corresponding to times longer than 10 min. These fits were extrapolated back to the begin point of the isotherms and define the isothermal baseline (shown as dashed lines in Fig. 1). Subtraction of these baselines from the corresponding measured traces yields the transient heat release, which can now be studied in detail (the transient heat release at the beginning of the isotherm can be used as a measure of the position of the baseline during scanned measurements, see Sec. IV).

Three different methods have been used to analyze the decay curves (see Table II). The first two (this section) are based on the idea that the heat release is due to the removal of defects from the network. At elevated temperature, defects may become mobile and disappear at traps, leading to unimolecular reaction kinetics characterized by an exponential decay with a single time constant. Alternatively, the defects may annihilate in pairs, leading to bimolecular reaction kinetics. The third method (following section) is in terms of activation energy spectra, a method commonly used to analyze structural relaxation in glasses.

Figure 2 shows the natural logarithm of the isothermal heat release decay signal as a function of time. In the figure, $t = 0$ corresponds to the position of the dotted lines in Fig. 1 and the curves have been offset for clarity. For longer times the data can be described by a straight line (not shown), but initially the decay is much faster. This could indicate that several processes, each with a different decay time, contribute to the heat release, or

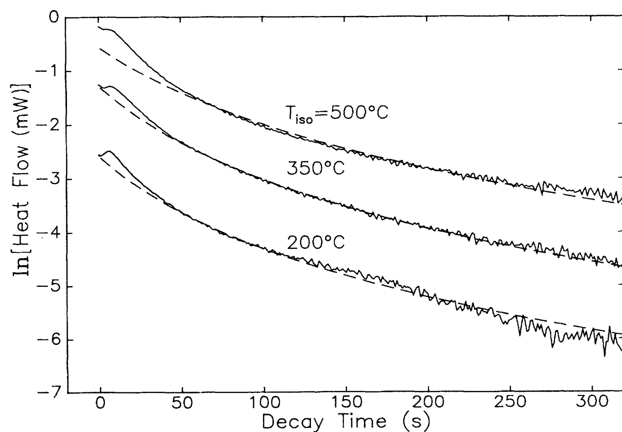

FIG. 2. DIC curves from Fig. 1, displayed on a logarithmic scale. Only the first 5 min are shown, and curves have been offset for clarity. Solid lines: data. Dashed lines: fits according to bimolecular reaction kinetics [Eq. (1)].

that the decay is not unimolecular. After the first processes have died out, the decay is dominated by the slowest process that still runs (at a measurable rate) at the temperature under consideration. The values for the characteristic time τ of these processes can be determined from the slope of the fits (not shown) and are found to be 113 ± 11, 107 ± 11, and 115 ± 12 s at 200 °C, 350 °C, and 500 °C, respectively (see Table II).

These values may be compared with those obtained by Donovan *et al.*[23] The magnitude of τ is about the same, but there is no temperature dependence, contrary to that found by Donovan *et al.* This difference is probably due to the fact that Donovan *et al.* determined all isotherms in one run of one set of samples. The measurements shown in Fig. 1 were each taken with a new set of samples. Therefore, samples used for the isotherms at higher temperatures have a different thermal history in both experiments. It is noted that the temperature dependence found by Donovan *et al.* is very weak.

A similar difference is observed when τ is compared with the transients determined using Raman spectroscopy.[21] These data showed a clear temperature dependence (τ varied from 3.5 to 220 s in the temperature range of 200 °C–600 °C). However, considerable differences in the heating and cooling rates of the two experiments exist and are probably responsible for the observed difference. An additional difference between the Raman study and the present DIC measurements lies in the use of heavily phosphorus implanted *a*-Si in the former.

In the case of bimolecular reaction kinetics, the defect density n decays according to $dn/dt = -kn^2$, where k is a constant. The solution is $n(t) = n_0/(1+kn_0t)$. Under the assumption that (at a certain temperature) each annihilation event produces the same amount of heat h_0, the heat flow dH/dt then amounts to

$$dH/dt = \frac{h_0 n_0^2 k}{(1+n_0kt)^2} \equiv \frac{h_0 n_0/\tau}{(1+t/\tau)^2} . \tag{1}$$

The dashed lines in Fig. 2 are fits to the data according to this expression. It is clear that the bimolecular reaction kinetics describe the data over a much larger range than would be possible with a straight line (i.e., unimolecular). The values for τ used in the fits are 74, 73, and 95 s at 200 °C, 350 °C, and 500 °C, respectively.

These fits show that the kinetics of structural relaxation can be well described by a mechanism of mutual defect annihilation. At this point it is not clear what kind of defects, nor how many are involved. This will be discussed in Sec. VIII. It is noted here that a study of the effect of structural relaxation on the viscosity of *a*-Si showed that the changes could be described by bimolecular reaction kinetics.[52]

B. Activation energy spectra

Structural relaxation in glasses is generally described by a spectrum of processes[53] according to an expression of the form[54]

$$P(t) = P_\infty + \sum_i P_i \exp(-t/\tau_i) , \tag{2}$$

where $P(t)$ is a measured property (e.g., the stored strain energy, the defect density, or the average bond-angle distortion), P_∞ and P_i are constant, and the characteristic times τ_i obey an Arrhenius-type behavior of the form

$$\tau_i = \tau_0 \exp(E_i/kT) . \quad (3)$$

In the latter expression, E_i is the activation energy of a process which exhibits a characteristic time τ_i for relaxation. Assuming that τ_0 is simply given by h/kT, with h and k the constants of Planck and Boltzmann, respectively, the above characteristic times can be used to estimate the activation energy of the dominant processes at each of the studied temperatures. Amorphous Si is not a glass,[55] but this theory is formulated for any system in which processes with a continuous range of activation energies can take place. It can therefore be applied to relaxation in any amorphous material and not only to glass. We will now examine the measured transients of structural relaxation in *a*-Si in the context of this formalism.

The activation energy spectra can be made visible by plotting the derivative of the heat flow with respect to $\ln(t)$ as a function of $kT\ln(kT/ht)$. This has been done as is shown in Fig. 3, which displays the isotherms from Fig. 1 in this fashion. It can be seen that at each of the three temperatures a different set of processes is probed. At a low temperature (200 °C), only processes with a low E_i are probed, because processes with a higher E_i do not proceed at a measurable rate. At higher temperatures (e.g., 500 °C), the processes with low E_i have long since been completed (remember that the temperature at which the isotherm is determined is approached at a slow rate of only 40 K/min) and only processes with a higher E_i contribute to the heat release. The distributions are centered around 1.35, 1.8, and 2.2 eV at 200 °C, 350 °C, and 500 °C, respectively.

The typical values for E_i may be compared with the known values of the activation energy for solid-phase epitaxial (SPE) crystallization, namely 2.7 eV.[23,56] The highest activation energy observed for relaxation (2.2 eV) is just below that for SPE which is a direct result of the temperature regimes in which they are observed being adjacent.

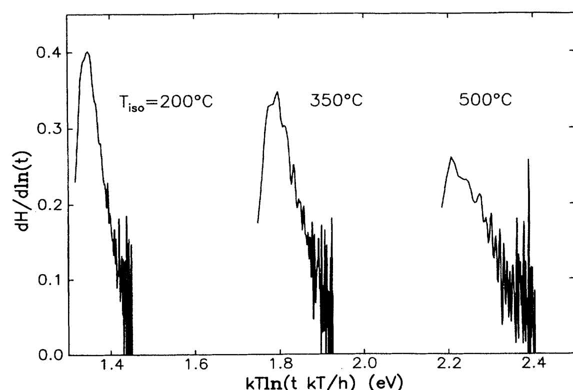

FIG. 3. Activation energy spectra, obtained from the DIC measurements shown in Fig. 1.

IV. STORED ENTHALPY DETERMINED BY SCANNING CALORIMETRY

A. Baseline correction procedure

Every DSC measurement characterizing irreversible processes consists in fact of two measurements: first a scan where the heat evolution due to the irreversible process under investigation is measured, followed by a scan of the same samples but now without the contribution of the irreversible process (which, by definition, occur only once). The problem is that the DSC instrument has a different thermal history during the two runs, and the thermal properties of the samples, especially the thermal conductivity, may be different during the two runs. In order to accurately determine the total amount of heat released upon structural relaxation, a careful baseline correction procedure has been used. This procedure is explained in detail in the following paragraphs.

Figure 4 shows DSC difference measurements from six sets of *a*-Si samples which have been preannealed in vacuum at different temperatures (T_a) for 45 min. Each set consisted of three disks implanted on both sides as described in Sec. II. The preanneal temperatures were 150 °C, 230 °C, 300 °C, 400 °C, and 500 °C. One set was not annealed (as-implanted). The curves in Fig. 4 are the DSC signal of the first scan of each set of samples minus the second scan. Curves are offset for clarity, and each curve has a number according to the chronological order in which the data were taken. The only correction to the data before plotting them in Fig. 4 is a small correction for instrumental baseline drift. This has been done as follows: the difference between the isothermal signals (after heat release due to relaxation has died out) of the first and second scan was measured (both at the beginning and end of the DSC scan). A correction for the drift can then be performed assuming the drift is linear with time during temperature ramping. This correction was on the or-

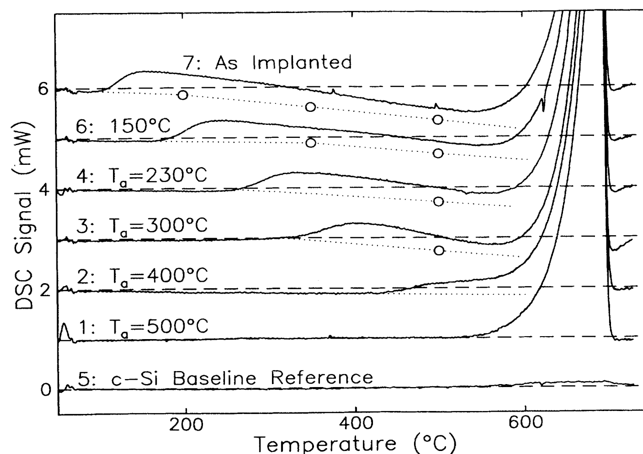

FIG. 4. DSC difference signal of *a*-Si for different preanneal temperatures (solid lines, curves are offset for clarity). Dashed lines: zero-signal baseline. Circles and dotted lines represent the position of the baseline deduced from isothermal measurements.

der of 0.1–0.2 mW. Curve number 5 (bottom) was measured with unimplanted c-Si disks loaded in both DSC pans and serves to indicate baseline stability and reliability of the baseline drift correction procedure. Dashed lines indicate zero-signal baselines, dotted lines will be discussed later.

Inspection of the curves in Fig. 4 shows that all traces from a-Si give a clear crystallization peak. Crystallization peaks run offscale because we chose to emphasize the smaller low-temperature signal. Curve 1, which was taken on a-Si preannealed at $T_a = 500\,^{\circ}\mathrm{C}$, does not deviate significantly from the zero-signal baseline until the temperature reaches $\approx 550\,^{\circ}\mathrm{C}$. Thus, the low-temperature thermal properties (specific heat, thermal conductivity, and variation of enthalpy) of a-Si preannealed at 500 °C are the same as those of c-Si (within the experimental accuracy). All other curves differ from curve 1 in three different ways. First, the signal clearly increases at a temperature which is about 50° above T_a, corresponding to the beginning of heat release accompanying structural relaxation. Second, the DSC signal deviates slightly but significantly from the zero-signal baseline at temperatures where one would expect the thermal properties of the samples to be the same as those of c-Si (i.e., below T_a). This can be seen most clearly for curve 2, although the effect is small compared to the magnitude of the other features.

Third, above T_a the DSC signal slowly decreases and even becomes negative. However, it should be noted that the isothermal measurements presented in Fig. 1 unambiguously show that an exothermic process is proceeding even at 500 °C. The apparent endothermic peak must therefore be due to a systematic baseline deviation. The position of the baseline at 200 °C, 350 °C, and 500 °C during the scanned measurements is known from the isothermal measurement shown in Fig. 1. The DIC signal is independent of baseline reproducibility.[23,57] The true baseline position is then such that the difference between baseline and signal corresponds to the isothermal heat release (at each of the temperatures) at $t = 0$. The values for this instantaneous heat flow, determined from Fig. 1, were 8.8, 7.5, and 5.6 ± 0.1 W/mol at 200 °C, 350 °C, and 500 °C, respectively. The baseline positions determined from these values have been indicated in Fig. 4 by circles. The dotted lines were fit to connect the circles and represent the corrected baseline. The difference between the solid and dotted lines is the total heat released by the a-Si during the first heating run. The corrected curves are plotted again in Fig. 5.

If the thermal conductivity of a-Si depends on the state of relaxation, this will influence the thermal gradient in the stack of Si disks during DSC measurements. Assuming that the baseline shift is due only to a change in the thermal conductivity κ of a-Si during the first run (i.e., as a consequence of relaxation) it is possible to estimate how large this change in κ needs to be. A simple heat-flow calculation shows that an increasing κ, varying between values on the order of 6 and 600 mW/cm K, would lead to the observed baseline shift. Measurements of κ in a-Si samples prepared by both ion implantation and vacuum evaporation range from 7 to 120 mW/cm K.[58] Similarly,

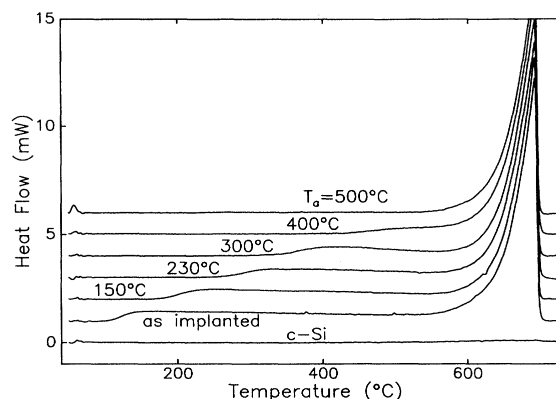

FIG. 5. Curves from Fig. 4 after baseline correction.

measurements of the thermal conductivity of a-Ge in different studies give results varying over almost two orders of magnitude[59–61] in the same range.

The variation in the reported values of κ for both a-Si and a-Ge,[58,59] combined with the observed baseline shifts in this study (Fig. 4), suggests that κ depends on the state of relaxation of a-Si. A possible mechanism could be a variation in the scattering of "phonons" from structural defects or density fluctuations in the network.[59,62] In addition to thermal conductivity effects, changes in the a-Si emissivity during DSC measurements may also contribute to the observed baseline shift.

B. Results: Heat release and crystallization velocity

The corrected curves shown in Fig. 5 can now be analyzed. A typical feature of the heat released from as-implanted a-Si which should be noted is the flatness of the curve over a wide temperature range. This is in agreement with the result from the isothermal decay curves, which show that many processes characterized by a spectrum of activation energies contribute to the relaxation signal. Curves taken on a-Si which had been preannealed at T_a show only a heat release for temperatures higher than $\approx 50\,^{\circ}\mathrm{C}$ above T_a. This has been found previously for relaxation in a-Ge (Refs. 63 and 64) and later in a-Si.[22,23,65]

The area under the curves in Fig. 5 can be integrated to yield the total heat released, H_{ac}, from both relaxation and crystallization of a-Si. This total enthalpy depends on the thermal history, i.e., the preanneal temperature T_a. Table III shows values for H_{ac}, determined from Fig. 5.[45] The values of 500 °C relaxed and as-implanted a-Si (13.7 ± 0.7 and 18.8 ± 1.0 kJ/mol, respectively) may be compared with earlier work when we found $H_{ac} = 11.7 \pm 1.0$ kJ/mol for 500 °C annealed a-Si and $H_{ac} = 15.4 \pm 1.0$ kJ/mol for as-implanted a-Si.[22] Considering that the earlier values are underestimates they are in good agreement with the present results. The heat release for the 500 °C annealed a-Si is not necessarily equal to the heat of crystallization (it has recently been found that rapid thermal annealing of a-Si at 700 °C and 800 °C relaxes it to a still lower quasiequilibrium state[66]).

TABLE III. Enthalpy difference H_{ac} between *a*-Si and *c*-Si, crystallization parameters, and Raman TO-like peak width $\Gamma/2$ for several *a*-Si preanneal temperatures.

Anneal temperature (°C)	Enthalpy H_{ac} (kJ/mol)	Enthalpy H_{cryst} (kJ/mol)	Crystallization velocity v_0 (10^6 m/s)	Crystallization velocity E_a (eV)	Raman $\Gamma/2$ (cm^{-1})
	18.8	13.5	6	2.33	43.2
150	18.3	14.0	17	2.42	41.5
230	17.1	13.5	7	2.35	40.6
300	15.8	13.5	28	2.46	39.2
400	15.2	14.0	12	2.39	36.8
500	13.7	13.5	35	2.48	34.1
average		13.7		2.41	

However, it is possible to separate the heat release due to crystallization from that due to relaxation, as will be shown in the following.

It has been well established that *a*-Si layers on a monocrystalline substrate regrow epitaxially and that the temperature dependence of the crystallization velocity v_c is characterized by an exponential with a single activation energy.[56] The heat release dH/dt due to crystallization during a DSC scan is the product of the amount of crystallized material and the (molar) heat of crystallization:

$$dH/dt = H_{\text{cryst}} v_c O/\rho \ , \qquad (4)$$

where H_{cryst} is the heat of crystallization, O the surface area of the *a*-Si layer, and ρ the molar volume. Since v_c can be written as $v_0 \exp(-E_a/kT)$, and keeping in mind that during a DSC scan the temperature is increased at a constant rate (of 40 K/min), it is seen that dH/dt is expected to behave as an exponential with a single activation energy and a prefactor $H_0 = H_{\text{cryst}} v_0 O/\rho$. Fitting an exponential to the rising slope of the peak determines H_0 and E_a. When the initial thickness of the *a*-Si layer is known, v_0 can be extracted from the constraint that the integrated regrown thickness equals the initial layer thickness at the temperature where the DSC signal comes back to 0. This method is similar to that used by Donovan *et al.*[64]

Each of the curves shown in Fig. 5 were fit by an exponential in the temperature region of 630 °C–690 °C and for each curve, E_a, v_0, and H_{cryst} were determined. One example of a measured curve and the exponential fit is shown in Fig. 6(a). The results of all curves are listed in Table III. It can be seen that the value for H_{cryst} is almost the same for all curves, showing that the fitted curves are essentially independent of the relaxation signal preceding the crystallization peak. The average value is $H_{\text{cryst}} = 13.7 \pm 0.3$ kJ/mol, which is very close to the value of 13.4 ± 0.7 kJ/mol of Donovan *et al.*[23] The average value of $E_a = 2.41$ eV is somewhat lower than that found by Donovan *et al.*

Using the values for E_a, v_0, and H_0, it is possible to compare directly the crystallization velocity measured by DSC with that measured by ion scattering and transient reflectance in combination with isothermal anneals.[56] Figure 6(b) shows the crystallization velocities in an Arrhenius fashion for two selected curves together with the

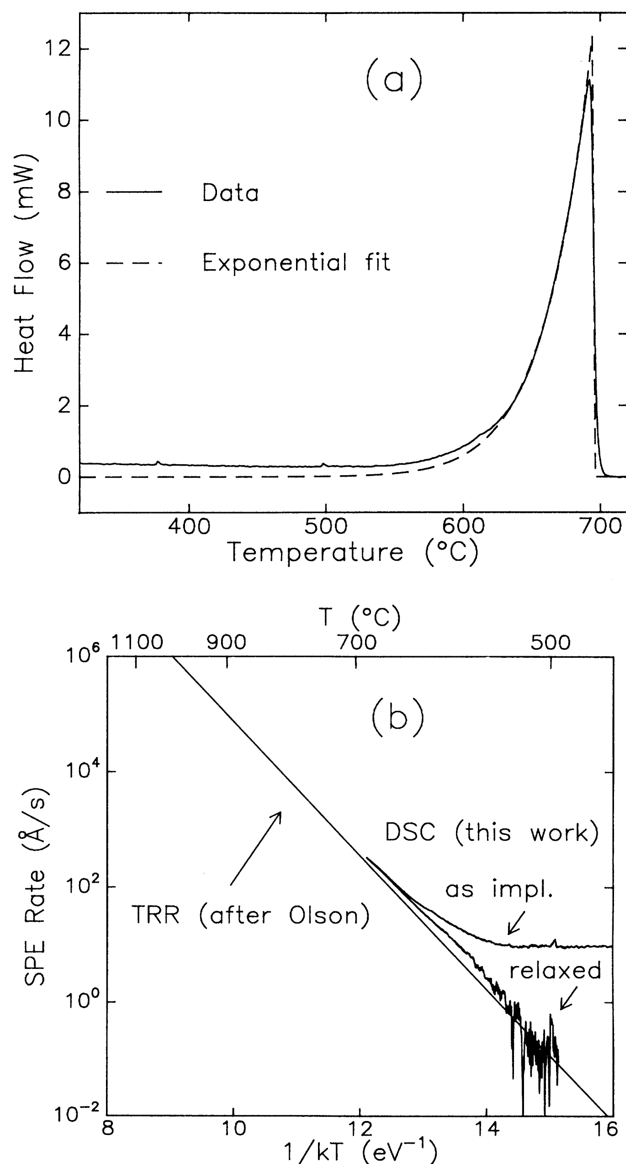

FIG. 6. (a) Measured DSC curve (solid line) and exponential fit (dashed line). (b) Two selected curves transformed to show crystallization velocity in an Arrhenius fashion and compared with transient reflectance measurements (Ref. 56).

data from Olson and Roth. It is seen that the crystallization velocities measured by DSC are somewhat higher and that E_a is lower than the value of Olson and Roth of 2.68 eV. The fact that we observe pure Arrhenius behavior for the crystallization signal does, however, validate the baseline correction procedure.

Table III also lists the half-width $\Gamma/2$ (at the high-energy side) of the transverse-optic-like (TO) band in the Raman spectrum of a-Si which received the same thermal treatment. It has been argued that a relation exists between the stored enthalpy in the a-Si network and $\Gamma/2$. This relation will be discussed in the following section.

V. STRUCTURAL ASPECTS OF RELAXATION

A. Relation between stored enthalpy and Raman spectroscopy

The Raman spectrum of disordered solids exhibits broadbands rather than narrow peaks because the momentum selection rules which govern Raman scattering in crystalline solids break down.[67] It has been suggested that the half-width $\Gamma/2$ of the TO-like band in the Raman spectrum of a-Si is dependent roughly linearly on the average bond-angle distortion $\Delta\Theta$ of the network[20,34,68,69] (however, from the pressure dependence of the a-Si Raman spectrum an inverse relation has been suggested to exist[70]). Furthermore the strain energy stored in the a-Si network can be related to $\Delta\Theta$.[71] Therefore, two possible relations between H_{ac} and $\Gamma/2$ may be envisioned.

(1) In a fully connected a-Si continuous random network (CRN), the excess enthalpy with respect to c-Si is expected to be mainly strain energy from bond angle distortions. For a Keating-type potential,[72] this energy is roughly proportional to the square of $\Delta\Theta$:[34,71]

$$H_{ac}=\sum 6[\tfrac{1}{2}k_{\Theta}(r\Delta\Theta)^2]\approx A(\Gamma/2-\Gamma_0)^2 \quad (5)$$

in which k_Θ is a bond-bending force constant and r is the Si-Si atomic distance (2.35 Å). The summation is over all atoms in the network, and the factor 6 represents the number of bond pairs per atom. k_Θ can be expressed in terms of the force constant β in Keating's potential[71,72] and may vary roughly between 6.7 and 9.7 N/m.[34,71,73,74] The prefactor A contains k_Θ, r^2, and a proportionality factor f describing the relation between $\Delta\Theta$ and $(\Gamma/2-\Gamma_0)$:

$$A=\sum 3k_{\Theta}r^2f^2 \ . \quad (6)$$

Beeman, Tsu, and Thorpe[68] calculate $\Gamma_0=7.4\ \text{cm}^{-1}$, and $f=3.2$ when $\Gamma/2$ is measured in cm^{-1} and $\Delta\Theta$ in degrees.

(2) Alternatively, a linear relation between the stored strain energy and $\Gamma/2$ may be found. From the data presented in Sec. VII it is suggested that a large concentration of complex point defects exists in a-Si and that these defects play an important role in structural relaxation. In general, point defects in Si are surrounded by small strained regions. To a first approximation $\Delta\Theta$ will then be proportional to the relative volume of strained material. As long as strained regions do not overlap, the volume of strained material will be proportional to the defect concentration. Thus $\Delta\Theta$ is a linear function of the number of point defects. Assuming that H_{ac} is the sum of the crystallization enthalpy H_{cryst} and a relaxation enthalpy H_{rel} proportional to the point-defect concentration, a linear relation then exists between $\Delta\Theta$ and $H_{\text{rel}}=H_{ac}-H_{\text{cryst}}$.

Figure 7 shows H_{ac} vs $\Gamma/2$ for a-Si, prepared by ion implantation followed by thermal anneal at different temperatures. In Fig. 7(a) the square root of H_{ac} is shown while Fig. 7(b) displays H_{rel}. Solid lines represent linear least-squares fits to the data points. The line shown in Fig. 7(a) corresponds to

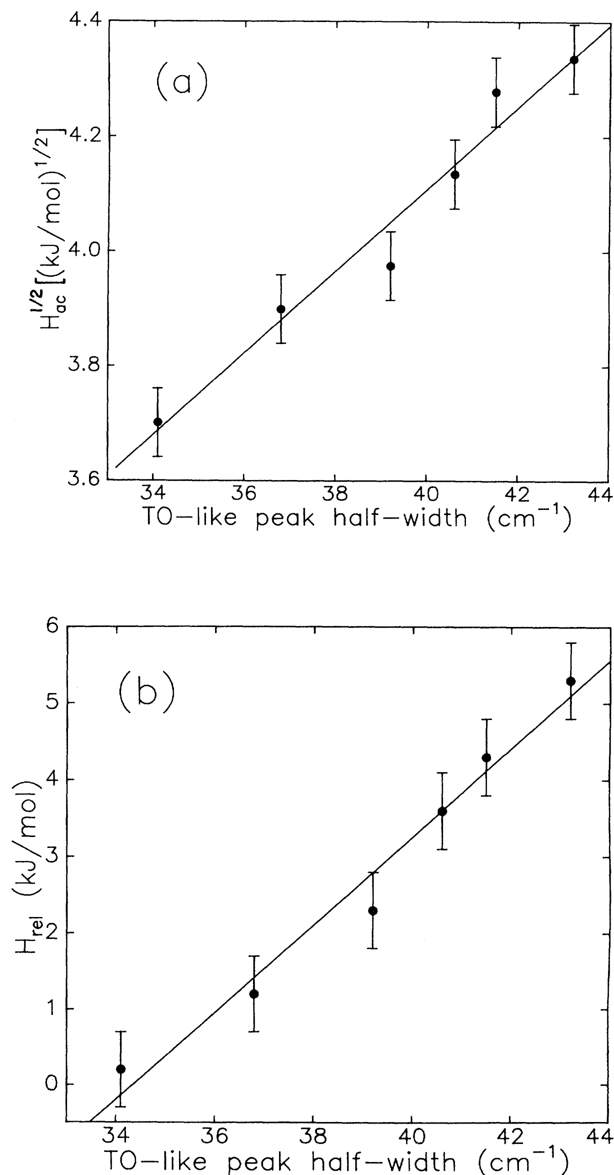

FIG. 7. Relation between Raman parameter $\Gamma/2$ and enthalpy difference H_{ac} for a-Si prepared by ion implantation followed by a thermal anneal at temperatures up to 500 °C. (a) Square root of H_{ac} vs $\Gamma/2$. (b) Excess enthalpy H_{rel} vs $\Gamma/2$. Solid lines represent least-squares linear fits to the data points.

$$(H_{ac})^{1/2}=0.071(\Gamma/2+17.6)\ , \qquad (7)$$

where H_{ac} is measured in kJ/mol and $\Gamma/2$ in cm^{-1}. This experimentally established relation may now be used to evaluate the present values for k_Θ and f. Assuming that the slope indeed represents the ratio of $\sqrt{k_\Theta}$ over f, then either k_Θ should be smaller (by at most a factor of 0.63) or f larger (by at most a factor of 1.3) than the previous estimates. However, the offset also differs from the predicted value, indicating that another contribution to H_{ac} may exist.

In Fig. 7(b), the relation between H_{rel} and $\Gamma/2$ is shown. The solid line is a linear least-squares fit which describes the data reasonably well. In the simplified picture (2) sketched above, the slope of 0.55 kJ cm/mol would correspond to the ratio $H_{def}/(\Gamma_{def}V_{def})$. Here, H_{def} represents the stored energy per defect (or defect cluster), Γ_{def} the local broadening in $\Gamma/2$ due to strained bonds in the neighborhood of the defect, and V_{def} the volume of the strained region. It is observed that the fits of Figs. 7(a) and 7(b) both describe the data points equally well. Consequently, neither of the aforementioned scenarios can be rejected on the basis of our results. It is emphasized that the relation found in Fig. 7(b) relies on the same physical interpretation of the relation between Raman peak width and distorted bonds, but with the extra ingredient that distorted bonds are localized in strained regions surrounding defects.

A relation between H_{ac} and $\Gamma/2$ has also been observed in a-Ge by Fortner and Lannin.[75] The Raman TO-like peak full width Γ was determined for a-Ge prepared by ion implantation and subsequent thermal treatments leading to (partial) relaxation. The peak widths were then compared to calorimetric measurements of the stored enthalpy reported previously by Donovan *et al.*[64] A linear dependence was found between $\sqrt{H_{rel}}$ and Γ. Analysis of their data as described above (i.e., $\sqrt{H_{ac}}$ or H_{rel} vs $\Gamma/2$) shows that the data can be equally well described with fits according to scenarios (1) and (2). Clearly a-Ge and a-Si behave very similarly in this respect.

B. X-ray diffraction

The variation in H_{ac} upon annealing has been related to ordering on an atomic level, involving a decrease in average bond-angle distortion $\Delta\Theta$ and/or removal of a large concentration of point-defect complexes. Such ordering involving many atoms is expected to result in changes in the x-ray-diffraction pattern of a-Si. This has indeed been observed, as shown in Fig. 8.

In Fig. 8 three XRD patterns are shown, corresponding to as-implanted, 230 °C, and 500 °C annealed a-Si. It can be seen that the patterns exhibit clear differences in the height and width of the first peak. The positions of the diffraction peaks are not affected by the anneal. The change in the intensity of the first peak corresponds to ordering on a scale beyond the nearest-neighbor distance. Analysis by Fourier transformation shows that the average nearest-neighbor distance does not change.

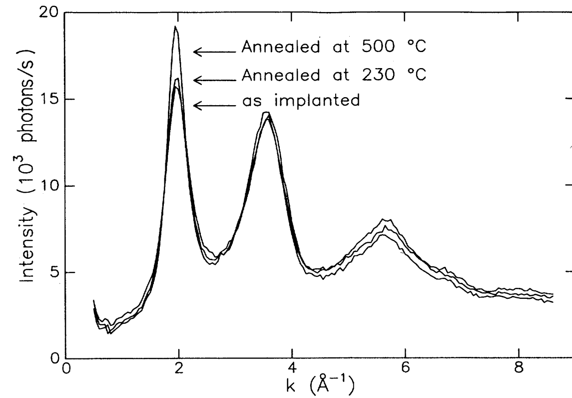

FIG. 8. X-ray-diffraction patterns of as-implanted and annealed a-Si.

The changes in the XRD pattern occurring upon relaxation of a-Si are very similar to those observed upon relaxation of a-Ge by both XRD (Ref. 76) and extended x-ray-absorption fine-structure (EXAFS) analysis.[77] In these studies, the changes could be related to a decrease in the average bond-angle distortion. It is concluded that annealing of a-Si indeed leads to reordering on an atomic level.

VI. AMORPHOUS Si PREPARED BY EVAPORATION AND LASER QUENCHING

A. Preparation techniques

The results in Secs. II–V show that the structure of a-Si, prepared by ion implantation (a-Si^{impl}), depends on the thermal history, as evidenced by measurements of enthalpy, Raman spectrum, and x-ray-diffraction pattern. Other methods of preparing pure a-Si exist however, and two of those will be investigated here. The purpose of this section is twofold: first, it is important to establish that relaxation is not merely an artifact of ion implantation, but a physical process typical of a-Si. Second, since different preparation methods result in different effective quenching rates, it is of interest to see whether "slow" quenching rates result in more relaxed a-Si than fast ones.

The two other methods of preparing pure a-Si which will be investigated in this section are e-gun evaporation[78] (a-Si^{evap}) and nanosecond[79–82] laser quenching from the melt (a-Si^{LQ}). It has already been shown by Raman spectroscopy that a-Si^{evap} and a-Si^{impl} are equivalent in terms of vibrational properties and that both materials show a decrease in the TO-like peak width upon annealing[19,21,83] characteristic of structural relaxation.[34] Raman spectroscopy has also been used previously to compare a-Si^{LQ} with chemical vapor deposition (CVD) deposited a-Si:H, showing that these materials are very similar.[84] An indication for the similarity of a-Si^{impl}, a-Si^{evap}, and a-Si^{LQ} is the fact that the activation energy and prefactor characterizing solid phase epitaxial regrowth of all three materials are the same within experimental accuracy.[56,85]

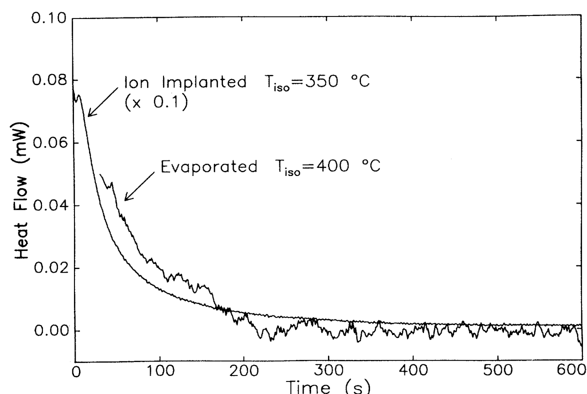

FIG. 9. DIC curves of a-Si prepared by vacuum evaporation and by ion implantation ($\times 0.1$).

B. Vacuum-deposited a-Si

Figure 9 shows two isotherms, one taken at a temperature of 400 °C on a-Si^{evap}, the other from ion-implanted a-Si at 350 °C. The amount of a-Si^{impl} in the DSC was 99.8 μmol, which is $\approx 10\times$as large as the amount of a-Si^{evap} that was used (11.6 μmol). Therefore the second isotherm has been scaled by a factor of 0.1. Both curves show a decaying positive signal, of about equal magnitude. This shows that a heat release upon heating for the first time occurs not only in a-Si^{impl}, but also in a-Si^{evap}. On the basis of DIC measurements, it can thus be concluded that structural relaxation, as observed in a-Si^{impl}, also occurs in a-Si^{evap}.

Raman spectroscopy confirms this conclusion. Table IV lists the position (λ_0) and half-width ($\Gamma/2$) of the main peak in the Raman spectrum of a-Si^{evap} before and after DSC analysis. Values for as-implanted and 400 °C relaxed a-Si^{impl} are also shown for comparison. The effect of relaxation is most clearly seen in $\Gamma/2$, which decreases from 40.5 to 37.6 cm^{-1} as the maximum temperature which the a-Si has been exposed to increases from 210 °C to 400 °C. This trend is similar to that in a-Si^{impl}, confirming the conclusion based on Fig. 9.

From the DSC and Raman spectroscopy comparison of vacuum-deposited and ion-implanted a-Si, it is concluded that structural relaxation is not an artifact of ion implantation but instead a process generally typical of a-Si. It will be seen in Sec. VII that annihilation of point defects plays an important role in structural relaxation of a-Si prepared by ion implantation. Clearly, any preparation method of a-Si is a highly nonequilibrium process making it possible to quench in a large concentration of defects. It is remarkable that a-Si formed in such different ways as by ion implantation and vacuum evaporation is so similar as far as vibrational and thermodynamic properties are concerned.

C. Laser-quenched a-Si

The properties of a-Si and the nature of the preparation method are intimately related, as a consequence of the nonequilibrium nature of a-Si itself. It is therefore interesting to investigate the structural state of a-Si^{LQ} prepared by rapid quenching of liquid Si (laser quenching). Laser quenching differs from ion implantation and vacuum deposition in that the a-Si resides at very high temperatures for a short period immediately following solidification.

The amount of laser-quenched a-Si which can in practice be prepared is insufficient for DSC analysis. Therefore, only Raman measurements were performed on a-Si^{LQ}, and compared with a-Si^{impl}. Spectra taken in HH polarization[20] are shown in Fig. 10 for a-Si^{LQ}, as-implanted a-Si^{impl}, and relaxed a-Si^{impl}. Only the spectrum from amorphized Si(111) is shown. Because the a-Si^{LQ} layers are thin relative to the penetration depth of the Raman probe laser there is a significant contribution to the spectra from the underlying c-Si substrate. The c-Si TO peak at 521 cm^{-1} prevented the width of the a-Si TO-like band to be determined accurately. The spectra shown in the figure have been scaled to equal intensity in the spectral region 560–600 cm^{-1}. The position of the maximum of the TO-like peak (λ_0) has been indicated for each curve. Both λ_0 and the height of the peak are different for all three curves. The peak of the laser-quenched sample may be reduced in intensity because of the limited thickness of the a-Si layer. The position, however, is sensitive only to the structure of the a-Si itself. For thinner a-Si^{LQ} layers on Si(100) substrates (not shown), the c-Si peak dominated the (HH) spectrum, but could be reduced in intensity by selecting vertically polarized outgoing light (VH). No differences in (VH) Raman spectrum were found between a-Si quenched on either (100) or (111) c-Si substrates.

Comparing λ_0 for a-Si^{LQ} with the values for relaxed (at 500 °C) and unrelaxed a-Si^{impl}, it can be seen that, according to Raman spectroscopy, laser-quenched material is (almost fully) *relaxed* a-Si. A similar conclusion has been drawn from a comparison of a-Si^{LQ} with CVD deposited a-Si:H.[84] Either the nature of the amorphization is such

TABLE IV. Raman TO-like peak position λ_0 and half-width $\Gamma/2$ for a-Si^{evap}, before and after DSC analysis. Values for a-Si^{impl} in unrelaxed and relaxed states are also shown.

Sample history	T_{max} (°C)	λ_0 (cm^{-1})	$\Gamma/2$ (cm^{-1})
a-Si^{evap}, as deposited	210	473.4	40.5
a-Si^{evap}, after DSC	400	475.9	37.6
a-Si^{impl}, as implanted	RT	470.4	43.2
a-Si^{impl}, relaxed	400	479.0	36.8

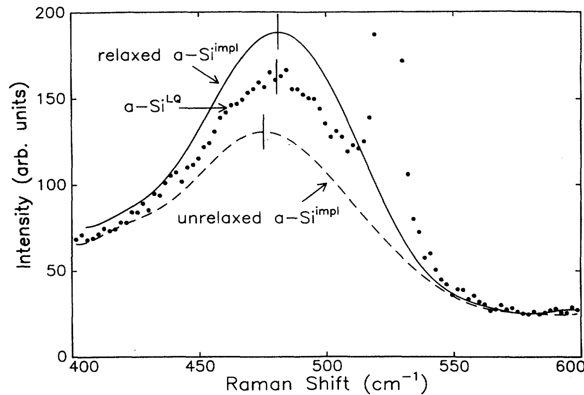

FIG. 10. Raman spectrum (TO-like band only) of laser-quenched a-Si compared with that of a-Si prepared by ion implantation. Both as-implanted as well as 500 °C relaxed a-Si are shown. Vertical lines serve to indicate peak position.

that relaxed a-Si is formed, or the freshly formed a-Si relaxes as it cools down. The latter case would imply that relaxation of a-Si at temperatures near its melting point[86] is fast on a nanosecond time scale.[87] It has recently been observed that rapid thermal annealing at 700 °C and 800 °C of a-Si leads within seconds to narrower Raman peaks than can be obtained by prolonged annealing at 600 °C.[66] Fast relaxation at high temperatures may explain why the melting temperature of a-Si appears to be only weakly dependent on the thermal history[86,88,89] contrary to what has been suggested[34] on the basis of the a-Si Gibbs free-energy diagram.

Returning to the subject of laser quenching of a-Si, it should be noted that a small change in the laser energy density, and consequently in the velocity and/or temperature of the freezing interface, can lead to the formation of c-Si.[81] Intuitively one would expect it to be unlikely that unrelaxed a-Si is formed when a minor change in treatment leads to c-Si. The crystal formed in this way is highly defective, with the defects typically being twins and dislocations when the irradiation conditions are close to the amorphization threshold.[81] Even when the laser conditions lead to a twin- and dislocation-free crystal can point defects be observed in the solidified c-Si layer.[90–93] If the defect densities are sufficiently high, this would imply that laser quenched a-Si, if it contains a similar amount of point defects, is formed in an unrelaxed state (see Secs. VII and VIII). It would be interesting to investigate the structure of a-Si formed by still faster quenching rates such as obtained in picosecond laser experiments,[94] which may result in somewhat higher solidification velocities and lower interface temperatures.

VII. DISPLACEMENT DAMAGE IN c-Si AND IN a-Si: DEFECT ANNIHILATION

A. Introduction

It has previously been established from the electrical,[95] luminescence,[12] and spin properties of a-Si (Ref. 10) that point defects exist in the network. Moreover, in the case of a-Si:H it has been established that the electrical properties are mainly controlled by point defects. Even though a-Si:H and a-Si are not identical, it raises immediately the question of to what extent structural relaxation in a-Si is controlled by defect annealing. This question will be addressed in this section.

Ion bombardment of a-Si:H has previously been used to introduce dopants[96,97] or to study radiation damage by, e.g., luminescence and ESR,[98] monitoring changes in electrical properties[99] or deep-level transient spectroscopy.[100] The results confirm that defects exist in a-Si:H. The connection between the annealing of defects and structural relaxation in pure a-Si remains to be established. It is not clear, for instance, whether annealing of defects involves the actual removal (annihilation) of the defects from the a-Si, clustering of defects to larger structures, or merely passivation by H. For annealing of metastable defects related to the Staebler-Wronski effect,[18,10] H diffusion has been shown to play a crucial role[102,103] indicating that, in this case, the defect structures are not removed from the a-Si:H but passivated. A second reason which makes it difficult to apply the results obtained from studies of bombarded a-Si:H to structural relaxation in a-Si is the fact that H atoms have a considerably higher cross section for displacement than Si atoms. It is to be expected that similar bombardments will lead to substantially more displacement damage in a-Si:H than in a-Si.

In this section, we study relaxed a-Si and c-Si, which have been simultaneously subjected to identical ion bombardments. The bombardment leads to ion-beam-induced damage in the material and this is studied using transmission electron microscopy (TEM) and Rutherford backscattering (RBS) (c-Si only) as well as Raman spectroscopy and differential scanning calorimetry (both a-Si and c-Si). Details of the ion bombardment treatments and Monte Carlo calculations of the amount of ion-beam-induced damage have been given in Sec. II. In this section the amount of damage in c-Si as a function of ion species, energy, and dose will be investigated. The damage dose necessary to saturate ion damage ("fully derelax") a-Si will be determined from changes in the Raman spectrum of a-Si. Finally the heat release upon annihilation of defects in c-Si, as measured by DSC, will be compared with the heat release from similarly damaged a-Si.

B. Ion-beam-induced damage in c-Si

1. Channeling studies

RBS analysis with one of the crystal axes parallel to the direction of the analyzing ion beam is known as channeling[104,105] and may be used to estimate the number of atoms which are off-lattice positions. The RBS-channeling spectra of He^+ bombarded c-Si are shown in Fig. 11. Figure 11(a) shows spectra taken before and 11(b) shows spectra after DSC analysis to a maximum temperature of 400 °C (results of which are reported below). A random spectrum and a channeled spectrum of unimplanted c-Si are shown for comparison. Four samples are shown, with ion fluences resulting in 0.03,

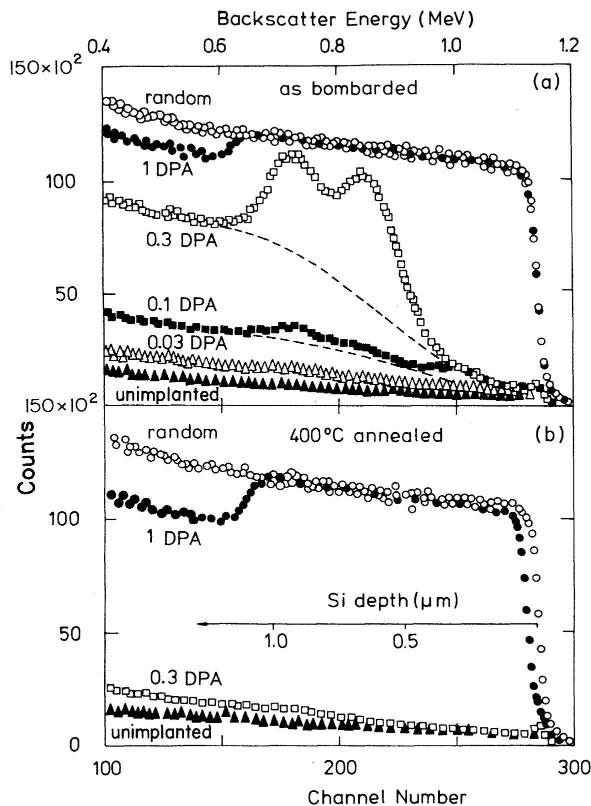

FIG. 11. RBS-channeling spectra of ion-bombarded c-Si (a) before and (b) after DSC.

0.1, 0.3, (120 and 200 keV only), and 1 DPA. The spectrum for 0.01 DPA (not shown) cannot be distinguished from that of unimplanted c-Si. The spectrum for 0.03 DPA is only slightly different from that of unimplanted Si, but the other spectra all show an increased yield, the curve for 1 DPA being indistinguishable from that of completely amorphized Si. It may be surprising that a He^+ implant to a dose of $\approx 2\times10^{17}$ ions/cm^2 is sufficient to amorphize Si. However, it is noted that the implants were performed with the targets held at 77 K which greatly reduces mobility and recombination of as-prepared defects so that much lower fluences are needed for amorphization in comparison to room-temperature implants.[106,107]

The number of displaced atoms can be estimated from the spectra in Fig. 11(a). The backscattered yield consists of two contributions, one due to direct scattering from atoms which are not on lattice positions and one due to dechanneling followed by scattering off atoms which are on lattice positions.[104,105] The contribution of dechanneling can be estimated (shown as a dashed line) and subtracted from the total yield, which gives an estimate for the number of displaced atoms. For 0.1 DPA this number is $\approx 3\times10^{17}$ cm^{-2}, and for 0.3 DPA, $\approx 1.3\times10^{18}$ cm^{-2}. These numbers may be compared with the Si areal density of a 1.2-μm-thick layer which is 6×10^{18} cm^{-2} and thus correspond to 5% and 20% displaced atoms, respectively. This is only a rough indication of the number of displaced atoms; the direct scattering cross sections for defects such as a divacancy are not known exactly and probably depend on the geometry of the defect itself as well as on the local lattice distortions due to the defect.

The RBS-channeling spectra after DSC analysis are shown in Fig. 11(b). Spectra for 0.03 and 0.1 DPA cannot be distinguished from the spectrum of unimplanted c-Si and are not shown. The damage causing the increased yield in Fig. 11(a) has disappeared except in case of the 1 DPA bombardment. Apparently 1 DPA suffices to amorphize Si completely (the shift of the leading edge indicates that the surface was not amorphized completely and recrystallized during the low-temperature DSC analysis). It appears, therefore, that an ion fluence corresponding to 0.3 DPA gives the maximum amount of damage which is unstable under heating to 400 °C.

2. *Electron microscopy*

Having established the amount of damage by RBS, it is useful to examine the same samples by TEM in order to determine the nature of the damage.[108] The 0.1 and 0.3 DPA samples (see Fig. 11) were investigated. Cross-section samples were prepared by mechanical polishing to $\approx 70-100$ μm and ion milling with 4-keV Ar^+ ions. In order to minimize surface damage the final stage was carried out at 1 keV. Some TEM was carried out at 200 keV, but the voltage was generally maintained below 150 keV in order to avoid electron-beam heating effects.

Figures 12(a) and 12(b) show transmission electron micrographs of cross sections of the 0.1 and 0.3 DPA c-Si samples, respectively. In these dark-field images at the (400) Bragg position strong contrast can be seen due to thickness fringes throughout the layers (which is particularly strong in the 0.3 DPA sample). In addition, the 0.3 DPA sample (implanted with 120- and 200-keV He^+ ions) shows a speckled appearance within two bands (near the bottom of the micrograph). Weak-beam microscopy has been used to show the presence of small (30–100 Å) strained regions within these damage bands, and selected area diffraction confirms that, as might be expected from previous studies of ion-beam amorphization, these regions consist of small amorphous zones. Further evidence for the amorphous nature of such clusters has recently been obtained; it was shown that the kinetics of ion-beam-induced annealing of such damage clusters are similar to those of ion-beam-induced epitaxial recrystallization of a-Si.[109]

In the 0.1 DPA c-Si sample, however, none of these amorphous zones are visible. Indeed, it is very difficult to distinguish the end-of-range damage of the He^+ ions in this sample, although a very faint band of diffuse contrast may just be made out (near the bottom of the micrograph). Since the dose is only a factor of 3 lower than that in Fig. 12(b), TEM does not appear to be consistent with a continuous buildup and overlap of individual collision cascades. Analysis by RBS and channeling of the 0.1 DPA sample revealed a ≈ 5 at. % density of direct scattering centers in the ≈ 1.2-μm-thick surface layer [Fig. 11(a)]. It is concluded that these scattering centers

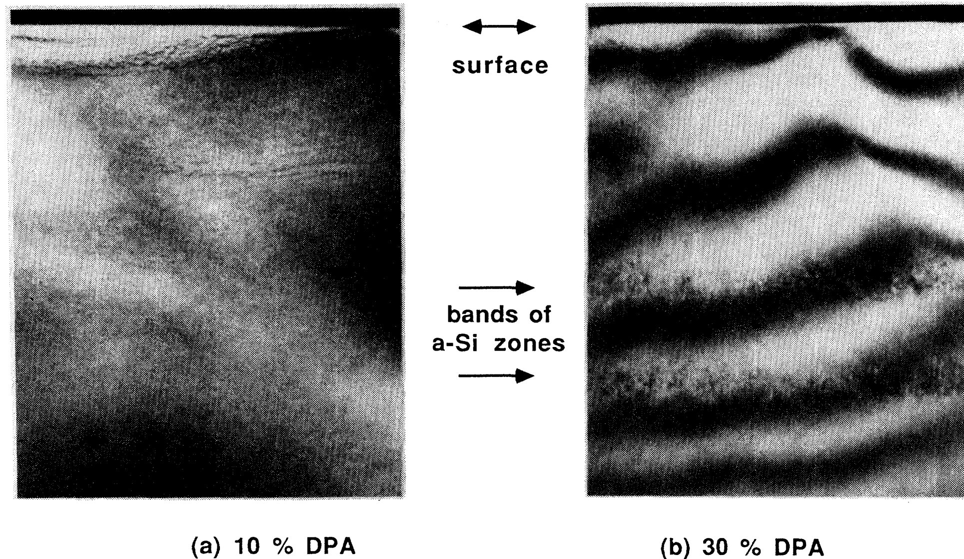

FIG. 12. TEM micrographs of (a) 0.1 DPA and (b) 0.3 DPA He^+-ion bombarded *c*-Si, before DSC measurements. Arrows indicate position of the surface and bands of defects.

are point defects that remain after recombination of vacancies and interstitials formed during the bombardment. Here, the term "point defect" is meant to include clusters of point defects that are too small to be observed in TEM.

The results shown in Figs. 11 and 12 are in agreement with the generally accepted view of ion damage in *c*-Si: energetic collisions between target atoms on lattice positions and the projectile or recoiled target atoms lead to the formation of vacancies and interstitials. These vacancies and interstitials are known to be mobile even at low temperatures and may either recombine or form larger point defects (e.g., divacancies and trivacancies) which are stable at room temperature.[110] Apparently there is a critical density of displaced atoms, above which point defects accumulate to form clusters, visible in TEM and finally resulting in a continuous amorphous layer. This behavior is consistent with the observation by Ruault and co-workers of a time delay in the formation of ion-beam-induced amorphous zones in heavy-ion irradiated *c*-Si.[111,112] The threshold density of displaced atoms is formed during irradiations (at 77 K) corresponding to 0.1–0.3 DPA.

3. *Raman spectroscopy*

In addition to RBS and TEM, Raman spectroscopy may be used to investigate the ion-beam-induced damage.[113–115] Figure 13 shows Raman spectra of untreated and He^+ bombarded *c*-Si (similar to those used for RBS and TEM). The spectrum for unimplanted *c*-Si (bottom) shows a sharp first-order peak at 521 cm^{-1}, second-order peaks near 300 and 440 cm^{-1}, and no signal below 200 cm^{-1}. The spectrum for ion-irradiated *c*-Si (middle) shows a broadening of the first-order peak as well as the appearance of signal at low wave numbers. These changes are indicative of distortions in the crystal lattice.[116] The intensity of the first-order peak has decreased which is most likely due to both a higher absorption in the damaged *c*-Si and broadening of the peak. The spectrum for Si bombarded with He^+ to a damage dose of 1 DPA (top) shows broad peaks near 150 and 470 cm^{-1} and weak features around 300 and 380 cm^{-1}. These features are characteristic of *a*-Si (Ref. 117) which confirms the conclusion based on Fig. 11 that the 1 DPA He^+ bombardment has amorphized the top layer of the

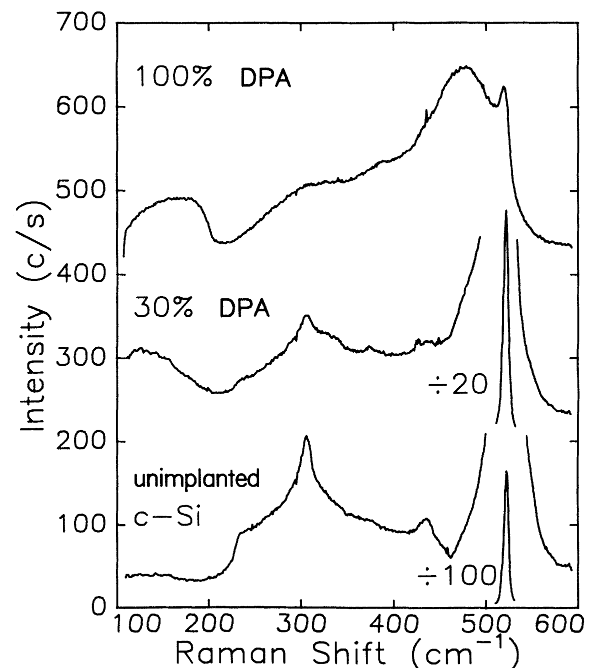

FIG. 13. Raman spectra of unimplanted *c*-Si (bottom) and of *c*-Si after bombardment with keV He^+ ions to a damage dose of 0.3 (middle) and 1.0 (top) DPA.

sample. The presence of the peak near 521 cm^{-1} shows the existence of *c*-Si at the surface. Note that the signal below 200 cm^{-1} is qualitatively different for *a*-Si and damaged *c*-Si.[116,118]

C. Ion-beam-induced damage in *a*-Si

1. Raman spectroscopy

Having established the effect of ion bombardment in *c*-Si, relaxed *a*-Si has been subjected to identical bombardment conditions. This makes it possible to directly compare ion damage in *a*-Si and in *c*-Si. Raman spectra of as-implanted, relaxed, and relaxed-and-bombarded *a*-Si are shown in Fig. 14. The position (λ_0) and half-width ($\Gamma/2$) of the TO-like peaks are indicated. It can be seen that λ_0 shifts to higher wave numbers and that $\Gamma/2$ decreases as a result of the anneal (compare the bottom and middle curve).[19–21] The top spectrum is that of relaxed *a*-Si which has been irradiated with 4.5-MeV, 5×10^{15} C^+/cm^2 ($\approx$0.04 DPA). This spectrum resembles that of as-implanted *a*-Si (bottom) indicating that the effect of the ion bombardment on relaxed *a*-Si is to return it to its unrelaxed state. In itself, this is not surprising because the *a*-Si was made by ion implantation in the first place. What is surprising is the ion dose at which this occurs: the dose required is namely much smaller than that needed for complete amorphization of *c*-Si (5×10^{16} C^+/cm^2). This has also been observed by infrared analysis of $^{29}Si^+$ implanted *a*-Si which had first been relaxed.[119]

Bombardment with different projectiles gives similar results when the ion doses are normalized to equal amounts of displacement damage (DPA). This is illustrated in Fig. 15, which shows the half-width $\Gamma/2$ (bottom) and position λ_0 (top) of the TO-like peak in the Raman spectrum of *relaxed a*-Si after C^+, Si^+, or Ge^+ ion bombardment as a function of damage dose. Increasing symbol size corresponds to increasing projectile mass. For comparison, the values for as-implanted and well-relaxed (45 min, 500 °C) *a*-Si are indicated. The ion dose is expressed in DPA as well as in ions/cm^2. It can be seen that for low ion doses $\Gamma/2$ and λ_0 resemble the values characteristic for well-relaxed *a*-Si, while for high doses $\Gamma/2$ and λ_0 resemble values of as-implanted *a*-Si. The transition from relaxed to unrelaxed occurs for ion doses on the order of $\approx$0.02 DPA, irrespective of the mass of the projectile. This is the critical dose for derelaxation.

When the three projectiles are compared on an equivalent DPA base, the amount of energy deposited in *a*-Si due to electronic stopping changes over two orders of magnitude (note that the dose in ions/cm^2, indicated on the top axis of Fig. 15, is very different for the different projectiles). Therefore it is clear that derelaxation of *a*-Si by ion beams is due to nuclear collisions. Since the major part of the transition has occurred for a dose of 0.05 DPA, it appears that only one out of every 20 Si atoms needs to be displaced by a violent collision in order to almost completely derelax the *a*-Si. This may again be compared with the damage that is necessary to completely amorphize *c*-Si, which is between 0.3 and 1

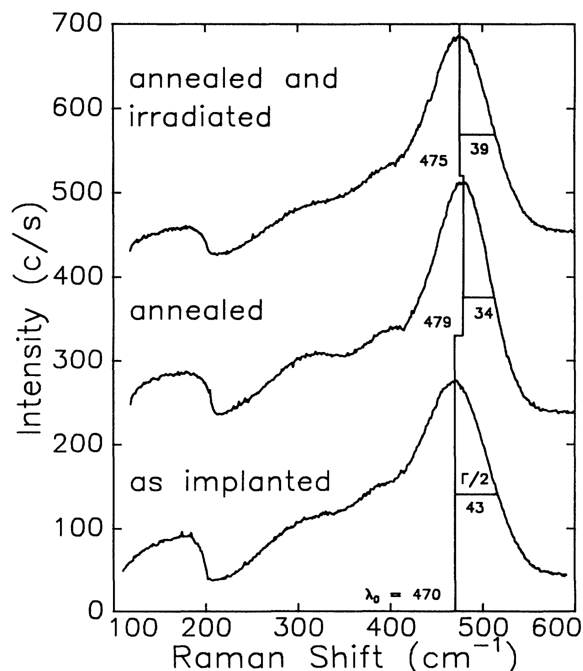

FIG. 14. Raman spectra of *a*-Si as implanted (bottom), after a thermal anneal at 500 °C for 45 min (middle), and after anneal followed by bombardment with MeV C^+ ions to a damage dose of $\approx$0.04 DPA (top).

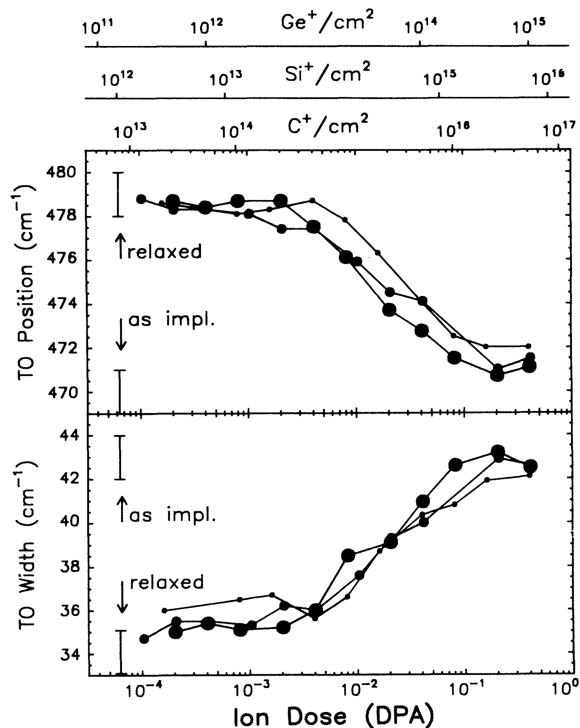

FIG. 15. Half-width (bottom) and position (top) of the TO-like Raman peak from annealed *a*-Si as a function of post-anneal ion irradiation dose. Increasing symbol size corresponds to increasing projectile mass for C^+, Si^+, and Ge^+ ions. Indicated are typical values for as-implanted and relaxed *a*-Si.

DPA under the irradiation conditions used here (see Figs. 11 and 13).

C. Calorimetric analysis of damage annealing in *a*-Si and *c*-Si

1. Scanning calorimetry

The annealing characteristics, determined by calorimetry, of bombardment damage in relaxed *a*-Si and in *c*-Si are now compared directly. Figure 16 shows the low-temperature DSC traces of (a) well-relaxed *a*-Si and (b) *c*-Si, after irradiation with He^+ ions for a range of ion fluences. The curves for less than 0.03 DPA did not differ significantly from the zero-signal baseline and are not shown. The curves for 0.03–1 DPA *a*-Si [Fig. 16(a)] deviate clearly from the baseline, and show a heat release similar to that observed when as-implanted *a*-Si is ramp heated for the first time[22,23] (see also Secs. III and IV). Saturation occurs between 0.03 and 0.1 DPA. Thus, bombardment with He^+ ions yielding 0.03 (or more) DPA in well-relaxed *a*-Si results in "derelaxation" of the *a*-Si, i.e., the *a*-Si returns to the unrelaxed state which cannot be distinguished from as-implanted *a*-Si. This confirms the similar conclusion based on Raman analysis of ion bombarded *a*-Si (see Figs. 14 and 15).

Traces from He^+ bombarded *c*-Si are shown in Fig. 16(b). The curve for 0.03 DPA is not significantly different from the baseline but the curve for 0.1 DPA indicates a heat release which is qualitatively similar to the signal from *a*-Si. This sample contains the damage which has been identified, on the basis of RBS and TEM results (Figs. 11 and 12), as a distribution of point defects and small point-defect clusters with no extended defects. After the DSC analysis to 400 °C the damage has disappeared leaving a perfect crystal (according to RBS-channeling; in TEM some dislocations may be found[120]). It is concluded, therefore, that the heat release for the 0.1 DPA *c*-Si is due to annihilation of point defects and small

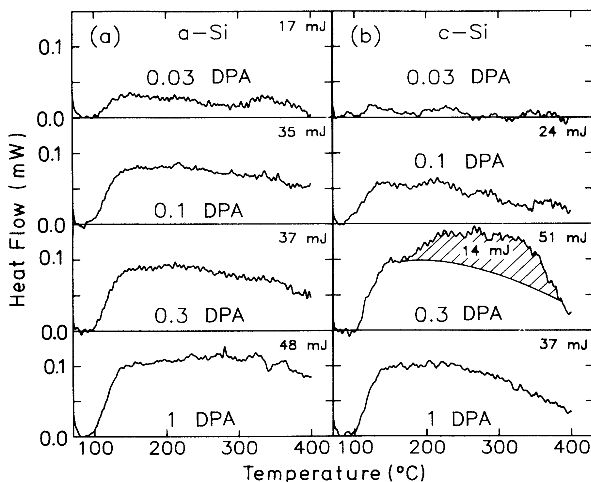

FIG. 16. Low-temperature DSC difference traces for (a) well-relaxed *a*-Si and (b) *c*-Si, after bombardment with keV He^+ ions. The hatched area is discussed in the text. The values of the integrated heat release are shown.

point-defect clusters only. These point defects seem to anneal out continuously over a range of temperatures, as opposed to annealing kinetics dominated by only a few processes (which would give rise to peaks in the DSC trace, compare Fig. 5). Such annealing behavior implies an assortment of point defects in irradiated *c*-Si, with a large number of routes to annihilation.[121–123]

The area under the DSC curve for 0.1 DPA *c*-Si, corresponding to the total amount of heat released, is 30% less than from 0.1 DPA *a*-Si. Combining the number of displaced atoms (5% in a 1.2-μm-thick surface layer according to RBS) with the integrated heat release (24 mJ from two 7.6-mm-diameter samples) gives 0.56 eV per displaced atom. This may serve as an estimate of the stored energy per defect, but it is emphasized that the number of displaced atoms as determined by RBS is not necessarily equal to the number of point defects.

For 1 DPA the signal from *c*-Si resembles that from *a*-Si, but with somewhat reduced magnitude. In fact, this is the dose where the sample has just been made amorphous (see Figs. 11 and 12) and the DSC signal is due to relaxation of this as-implanted *a*-Si. The curve for 0.3 DPA *c*-Si, which contains bands of amorphous zones (Figs. 11 and 12), differs from all other curves: a heat release can be seen which is larger than any other. Moreover, this curve is qualitatively different because above 180 °C an extra heat release begins (hatched area), which can be understood in terms of recrystallization of amorphous zones at anomalously low temperatures.

The assumption is made that the heat release from 0.3 DPA *c*-Si is a linear superposition of annihilation of point defects (i.e., 0.56 eV/displaced atom) and heat release from relaxation and crystallization of amorphous zones (0.12–0.16 eV/atom[22,23]). The contribution from point-defect annihilation should have the same onset and form as that from 0.1 DPA *c*-Si. The hatched area, therefore, corresponds to heat release from amorphous zones. From the measured heat release, the hatched area in Fig. 16 would then correspond to $(8.2-6.2)\times 10^{17}$ atoms/cm^2 and the remaining area to 4.6×10^{17} displaced atoms/cm^2, thus giving a total number of $(1.3-1.1)\times 10^{18}$ displaced atoms/cm^2. This number is in good agreement with the channeling estimate of 1.3×10^{18} cm^{-2} (Fig. 11). It is remarkable that the onset of epitaxial recrystallization in the 0.3 DPA *c*-Si occurs at 180 °C, but recrystallization of small amorphous zones at these low temperatures has been reported before.[111] One possible reason for this phenomenon is that these small amorphous zones are embedded in a sea of defects which can enhance crystallization.[124]

2. Isothermal calorimetry

Figure 17 shows DIC difference curves for 0.1 DPA *c*-Si (solid line) and *a*-Si (dashed line), measured at 400 °C (the *a*-Si signal has been divided by 2). Apart from a difference in magnitude the curves are similar, and both curves are similar to that of structural relaxation of *a*-Si (see Figs. 2 and 9). Moreover, both curves can be described by bimolecular reaction kinetics. The thick solid line represents Eq. (1), calculated with a characteristic

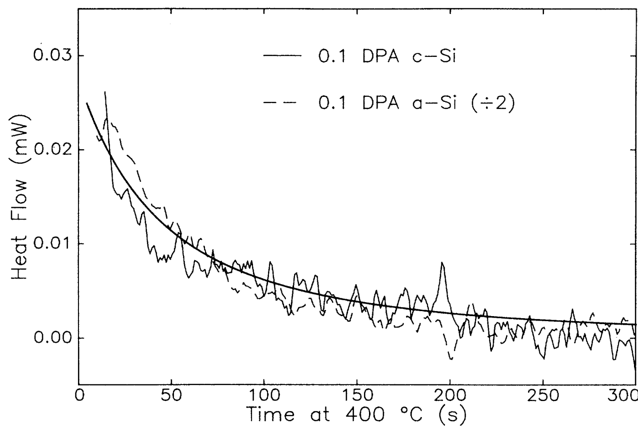

FIG. 17. Isothermal difference (DIC) signal for damage annealing in 0.1 DPA ion-bombardment Si. Solid line: heat release decay curve from crystalline Si. Dashed curve: heat release decay curve from amorphous Si. Thick solid line: decay according to bimolecular reaction kinetics [Eq. (1)].

time of 90 s (see Fig. 2 and Sec. III A).

Alternatively, the similarity between the kinetics of defect annihilation in *c*-Si (solid curve) and *a*-Si (dashed curve) can be taken to indicate that defect annihilation in *c*-Si can be characterized with a distribution of activated processes as has also been shown to be the case for structural relaxation of *a*-Si (see Fig. 3). This has in fact been observed before, as the annealing time of irradiated *c*-Si obeys a Meyer-Neldel rule.[122] It can also be inferred from DSC which shows a broad featureless curve with no sharp peaks.

Apart from a difference in magnitude similar to that in Fig. 16, the two curves in Fig. 17 are remarkably similar. Because the *a*-Si was subjected to exactly the same ion bombardment conditions as the *c*-Si, it is tempting to suggest that the heat release from both materials has a common cause. Moreover, the similarity with the decay curves shown in Fig. 9 taken on as-implanted and vacuum-evaporated *a*-Si (Fig. 9) suggests that this common cause is the same mechanism underlying structural relaxation in *a*-Si.

3. *Nuclear versus electronic energy losses*

The integrated heat release for each of the curves in Fig. 16 is plotted as a function of damage dose in Fig. 18(a). In addition, Figs. 18(b) and 18(c) show the total integrated heat release measured on Si^+ and Ge^+ bombarded Si. In the figure, solid circles represent data from relaxed-and-bombarded *a*-Si, while open circles represent measurements taken on bombarded *c*-Si. Once again the ion dose has been multiplied by the density of displaced target atoms per incident ion to yield the damage dose in DPA.

It can be seen that in all cases 0.03 DPA is the minimum damage necessary to induce a heat release, and the heat release from *a*-Si is larger than that from *c*-Si except for the 0.3 DPA bombardments. We recall that the heat release from 0.3 DPA He^+ bombarded *c*-Si shown in Fig. 16 is due to both point-defect annihilation and recrystallization of amorphous zones, whereas for other

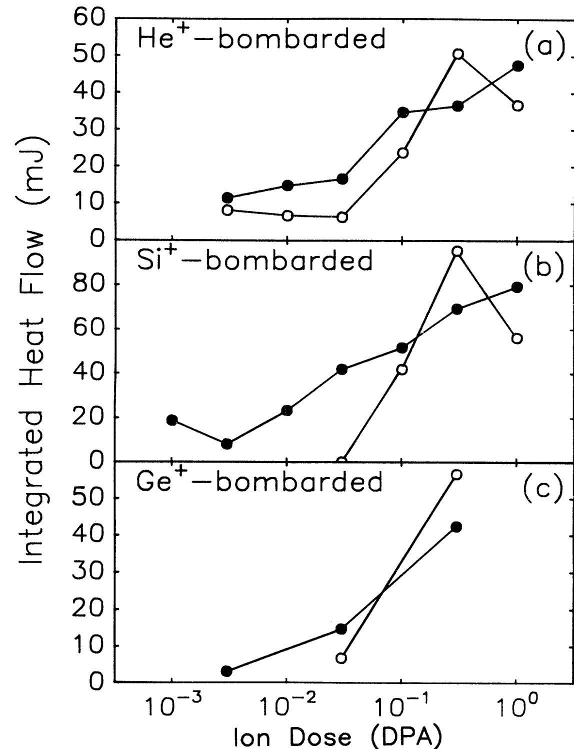

FIG. 18. Integrated heat release from relaxed and then (a) He^+, (b) Si^+, and (c) Ge^+ bombarded *a*-Si (solid circles) and *c*-Si (open circles) as a function of the ion fluence. The amount of defected material in the DSC was ≈ 9.1 μmol for (a) and 15.1 μmol for (b) and (c).

damage doses the heat release is solely due to point-defect annihilation or structural relaxation. It is now seen that for Si^+ and Ge^+ bombarded Si a similar trend exists: the 0.3 DPA bombardments stand out only because there is the heat release from *c*-Si larger than from *a*-Si. Moreover, the shape of the DSC traces obtained from Si^+ and Ge^+ bombarded Si were similar to that of structural relaxation, except for the 0.3 DPA *c*-Si traces which showed a signal similar to that of He^+ bombarded *c*-Si (Fig. 16). Thus, the results shown in Fig. 16 can be fully reproduced using Si^+ or Ge^+ bombardment, as long as the ion doses are scaled to the ion-beam-induced damage. This confirms the conclusion from the Raman measurements (Fig. 15) that ion-beam-induced derelaxation of *a*-Si is due to nuclear energy-loss processes rather than to electronic energy-loss mechanisms.

VIII. DISCUSSION: NATURE OF STRUCTURAL RELAXATION

A. Defect annihilation

In this section we will provide a more detailed interpretation of "structural relaxation" or "short-range ordering" in *a*-Si. By structural relaxation we mean the intrinsic network rearrangement (not collapse of macroscopic voids) accompanied by large changes in vibrational, structural, and thermodynamic properties. It is to be expected that defect annealing occurs when *a*-Si is heated

for the first time,[95] but it is not clear *a priori* whether relaxation and defect annealing are independent or related processes. It has been suggested, for example, that the structure of defects in *a*-Si (including its surroundings) depend on the short-range order in the network.[35] In this view the network is able to rearrange itself while the defects remain in place and become embedded in a progressively more ordered network as relaxation proceeds.

We now compare the DSC data associated with defect annihilation in ion-bombarded *c*-Si, with those of identically treated relaxed *a*-Si and of structural relaxation in *a*-Si. The traces of 0.1 DPA *a*-Si and *c*-Si [Figs. 16(a) and 16(b), and Fig. 17] are very similar, and peaks are absent on both curves. This suggests a common mechanism for annihilation of a large population of point defects in *c*-Si and damage removal in *a*-Si. Moreover, both traces are similar to that of structural relaxation of as-implanted *a*-Si [bottom trace for 1 DPA *c*-Si in Fig. 16(b), and Fig. 1]. Finally, the kinetics of damage removal in 0.1 DPA *a*-Si and *c*-Si, as reflected by the isothermal DSC curves shown in Fig. 17, appear very similar. In view of the fact that *a*- and *c*-Si are two very similar condensed phases of Si, both being held together by directional bonding and both fourfold coordinated, we conclude that apparently similar physical processes are going on in these materials. The atomic motion necessary for structural relaxation in *a*-Si appears to be similar to those of defect annihilation in *c*-Si. To put it more strongly, the data suggest that structural relaxation of *a*-Si *is* defect annihilation. Structural relaxation is not typical just of *a*-Si,[34,35] but also occurs in heavily damaged *c*-Si where it has long been known as defect annihilation.

The structure of the defects involved is expected to be similar (but not identical) to that of the defect population in heavily ion-damaged (but still crystalline) *c*-Si. Simple point defects can as easily be defined in a perfect, fully connected random network as in a perfect crystal lattice; for example, a divacancy is a defect consisting of two neighboring atoms missing. It is expected that in both *a*- and *c*-Si the atoms surrounding a defect slightly change their positions to accommodate the energetically highly unfavorable situation. This leads to bond-angle variations, and a large fraction of the energy associated with the defect is thought to be stored in these distorted bonds. The heat release observed during defect annihilation is therefore expected to be due to the change in structure around the collapsing defect in both *a*- and *c*-Si.

The suggestion that point-defect annihilation completely controls structural relaxation is further based on the observation (Fig. 2) that the isothermal heat release curves obey bimolecular reaction kinetics and on the observation (Figs. 15 and 18) that the ion-beam-induced derelaxation scales with the density of displaced atoms due to the ion bombardment and appears to be independent of electronic energy-loss mechanisms.

A rough estimate of the defect densities involved in structural relaxation can be made by comparing the integrated heat release from 0.03 and 0.1 DPA *a*-Si [Fig. 16(a)] with the formation enthalpy of the vacancy in *c*-Si, 3.6 eV.[125] Under the assumption that the average heat release from one annihilation event in *a*-Si is of the same order, this yields 0.5 ± 0.3 and 1.1 ± 0.6 at. % defects in 0.03 and 0.1 DPA *a*-Si, respectively. The relative error in this estimate comes from the large uncertainty ($\pm50\%$) introduced from the DSC baseline subtraction.

It is tempting to compare the magnitude of the saturated heat release in 0.1 DPA *a*-Si (35 mJ) with the "background" heat release related to point-defect annihilation in 0.3 *c*-Si of 37 mJ. Assuming that the amount of heat released per defect annihilation event is similar in *a*-Si and *c*-Si, it appears that the maximum amount of defects which can be sustained in Si at room temperature is similar in *a*-Si and *c*-Si.

When the role of short-range order in *a*-Si is discussed, it is generally pointed out that the properties of the *a*-Si depend on the short-range order (or state of relaxation) while the properties of *c*-Si do not depend on its thermal history. This is not true, however, for *c*-Si containing defects. In fact, many properties of *c*-Si are defect controlled (e.g., conductivity, mechanical strength, optical properties, and impurity diffusion). Defects, which have been introduced by means of highly nonequilibrium processes and can be annealed by thermal treatments, then introduce a similar thermal history dependence as observed in *a*-Si.

Defects in *a*-Si have been studied extensively with electron-spin-resonance (ESR) methods. In this method, unpaired electrons (or uncharged dangling bonds) give rise to a paramagnetic resonance which can be detected. Large spin densities up to 10^{20} cm^{-3} (Ref. 10) have been measured in deposited *a*-Si, but in *a*-Si prepared by ion implantation the maximum spin density observed is 2×10^{19} cm^{-3}.[11] Most of these spins anneal out during heating. However, in the first case[10] (at least a fraction of) the spins have been associated with dangling bonds on internal surfaces and voids of the kind that are manifestly absent in our ion-implanted films (as evidenced by the absence of a measurable density change upon relaxation[33]). In the second case,[11] the number of spins is much too low to account for the observed heat release[22] when it is assumed that every defect gives rise to one spin, as is seen in the following.

When ion-implanted *a*-Si is heated to 500 °C for the first time, it releases an amount of heat equal to about 5 kJ/mol. In addition, the ESR spin density is reduced by about 1×10^{19} cm^{-3}.[11] If the heat release is due to the removal of these dangling bonds only, then each dangling bond would have to contribute about 250 eV. This is clearly unphysical and therefore there must be another source. This source is either an unidentified structural relaxation mechanism unrelated to defect structures or removal of defects other than those that can be seen by ESR. We suggest the second possibility which implies that the majority of the defects cannot be detected by ESR. The discrepancy between ESR and DSC estimates of defect densities will be discussed in the following section together with other recent, related experimental results.

B. Total defect density in unrelaxed amorphous silicon

Although it has long been realized that structural defects similar to those in irradiated *c*-Si may be present in

a-Si (see, e.g., Ref. 95), the suggestion that structural relaxation in a-Si is fully defect controlled is new. It has led to new investigations[126–128] of defect structures in a-Si, probed by impurity diffusion and solubility measurements. These studies confirm both qualitatively and quantitatively the above picture of structural relaxation in terms of defect annihilation.

It has been established[129–131] that Cu, Ag, and Au are fast diffusers in a-Si and moreover that there is a remarkable correlation between diffusion in a- and c-Si in both absolute magnitude and activation energy. It can be generally stated[132] that the fast diffusers in c-Si, with interstitial components, are fast diffusers in a-Si and that the slow, substitutional diffusers in c-Si are also slow in a-Si. The solubility of fast diffusing species in a-Si was found to be at least six orders of magnitude greater than their solubility in c-Si. It is known that these species can be trapped or gettered at defects in c-Si, which means that the presence of defects in c-Si leads to a higher effective solubility. The new results show that both the diffusivity and the solubility of fast diffusers in a-Si depends on the state of relaxation in a manner which is consistent with the defect annihilation picture of structural relaxation sketched above.

It was found initially that the diffusivity of Cu in relaxed a-Si (annealed at 500 °C) is a factor of 2–5 higher than in unrelaxed a-Si but that the activation energy is not significantly different.[126] In this study, Cu was ion implanted at low energy into a 2-μm-thick layer of relaxed a-Si, leading to the formation of a 300-nm-thick unrelaxed a-Si surface layer. At the annealed-reimplanted phase boundary solute partitioning was observed, the partition coefficient being about 8. These results were interpreted to indicate that as-implanted a-Si contains a large number of traps. Annealing leads to a reduction in the trap density, and therefore also to a reduction in the effective solubility (hence the solute partitioning). A second effect of a reduced trap density is that the mean distance between traps becomes larger, which is consistent with an increased diffusivity.

More recently, quantitative agreement was found between the estimate of the total defect density in this paper and that based on diffusivity and solubility measurements. Pd ions were implanted in a-Si and redistributed over the entire a-Si layer thickness by annealing at 500 °C.[127] Subsequently, defects were introduced into the surface region by 200-keV Si^+-ion implantation at various doses. After diffusion at 250 °C, Pd atoms behaved similar to Pd in defected c-Si and were found to getter in the Si^+-ion implanted region. At low Si^+-ion fluences, Pd decorates the Gaussian depth distribution of the ion-induced damage, while at higher fluences a saturation is reached in the gettering profile. Saturation occurs at damage levels of $\approx$0.02 DPA, in agreement with the DSC and Raman results (Figs. 15 and 16). Moreover, quantitative analysis of the Pd diffusivity in a-Si yields, under the assumption that the diffusivity in trap-free a-Si equals that in c-Si, a density of defects acting as traps in as-implanted a-Si of $\approx$1 at. %.[128] This number is in good agreement with the value for the total defect concentration deduced from the heat of relaxation and the vacancy formation enthalpy, 1.1 at. %.

The diffusivity and solubility results and the quantitative agreement with the defect density determined from DSC provide strong evidence for the contention that structural relaxation in a-Si is in fact defect annihilation. It is emphasized that in metallic glasses the effect of structural relaxation on impurity diffusion is opposite to that observed in a-Si.[133] Therefore the concept of point defects acting as traps for the diffusing species is essential for the interpretation of the data.

There are several reports in the literature of estimated defect densities in a-Si by yet other techniques. Heidemann, Grüner, and te Kaat[134] measured optical profiles of beveled samples which were prepared by Si^+- or H^+-ion implantation of both as-implanted and annealed a-Si. The optical active site was believed to be a Si bonding defect (either a broken or a heavily strained bond), and the density of such sites in as-implanted a-Si was found to be 8 at. %. If more than one bonding defect is associated with a structural defect then this number would be an overestimate of the defect density. A study of positron annihilation in ion-implanted Si employing a variable energy slow positron beam and (Doppler broadening) line-shape analysis can also be understood in terms of defects. Vacancy-type defects may trap positrons and the spectra of a-Si could not be distinguished from c-Si containing "a few at. % defects."[135]

The total defect concentration in as-implanted a-Si as determined by any of the above-mentioned techniques (i.e., $\approx$1 at. %) is more than an order of magnitude higher than the spin density measured by ESR ($\approx$0.04 at. %, see Ref. 11). It appears, therefore, that ESR has a very limited sensitivity and is incapable of detecting the majority of the defects in a-Si. The limited sensitivity probably arises because ESR detects unpaired dangling bonds which have a large formation energy of several eV.[136] Consequently, the majority of the dangling bonds is expected to exchange electrons in pairs and become either positively or negatively charged,[136] thereby losing its ESR activity.

C. Defect annihilation and variable short-range order

At first sight the suggestion that structural relaxation is controlled entirely by defects may seem to contradict the initial interpretation in terms of average properties such as a short-range ordering or a decrease in the average bond-angle distortion.[19–21] It is noted, however, that defects are accompanied by a strain field due to small local rearrangements involving bond-angle distortions.[137] The extent of these lattice relaxations is not exactly known. For a first-order estimate it is useful to note that large effects have been reported for surface reconstruction of c-Si. The Si(111)7×7 reconstruction, for example, involves displacements which are noticeable five atomic layers deep and where even in layers close to the bulk, bond-angle deviations may be as large as 12°.[138] Calculations show that atoms neighboring a neutral monovacancy may be displaced 3% of a bond length inward.[139] A point-defect concentration of 1 at. % corresponds to an average distance between defects of about four interatomic spacings. Assuming that a point defect leads to small

local rearrangements of both nearest and next-nearest neighbors, it follows that these defect concentrations lead to distortion of a majority of bond angles.

This interpretation not only provides a more detailed picture of structural relaxation of *a*-Si, it also suggests that the population of point defects in *a*-Si is similar to that in *c*-Si. Both single vacancies and interstitials as well as small clusters of defects can easily be defined in a fully connected *a*-Si network without any need for the translational or rotational symmetry exhibited by the *c*-Si lattice. The possible existence of stable single vacancies and small vacancy clusters in a fourfold covalently bonded CRN has been predicted from calculations based on the Keating potential.[140] Based on measurements of electrical properties and annealing studies, the divacancy has been suggested to exist in *a*-Si:H.[95]

The fact that the density of *a*-Si remains unchanged upon relaxation[33] puts some limits on the nature of the defect annihilation process: it suggests mutual annihilation of low- and high-density defects. The simplest form of such a process is vacancy-interstitial recombination which probably already occurs at very low temperatures[137] and has only a small effect on the atomic density.[141]

With the suggestion that point-defect populations in *a*-Si and *c*-Si are similar we do not mean to state that they are identical. Clear differences are single dangling (or floating) bonds, which cannot exist in *c*-Si but are likely to be present in *a*-Si (and need substantial rearrangement of the network to be removed). Another difference occurs when defect clusters in *c*-Si become so large that the translational symmetry in the crystalline matrix becomes crucial for the structure of the cluster. An example could be dislocation loops in *c*-Si which may be thought of as a large cluster of interstitials.

D. Relaxation and defect processes in hydrogenated amorphous silicon

A material closely related to pure *a*-Si is hydrogenated *a*-Si (*a*-Si:H).[142] In *a*-Si:H, reversible changes in the conductivity have been observed.[18,101] The changes have been attributed to the creation and annealing of a population of metastable defects, possibly dangling[143] or floating[144,145] bonds, intrinsic to the *a*-Si:H network.[146] (Metastable-defect annealing will be referred to as MDA.) It has been shown that the kinetics of both MDA (Ref. 102) and defect creation[147] can be described as stretched exponentials (SE) or *b* functions.[148–150] Studies of diffusion of hydrogen in *a*-Si:H have shown that the H diffusivity at a certain temperature decreases with time[102,151] (which is called dispersive diffusion) and can also be described by a SE.[102] Moreover, the temperature dependence of the SE parameters describing both MDA and H diffusion exhibit a striking similarity. This has been interpreted as evidence that MDA is the result of passivation of localized defect states by H diffusing through the *a*-Si:H network.[102,103] A similar conclusion has been reached regarding the relation between creation of metastable defects and H diffusion.[152,153]

In the experiments described in this paper we are dealing exclusively with pure, unhydrogenated *a*-Si. Defect passivation by H can therefore be ruled out as a mechanism contributing to structural relaxation. Structural relaxation does, however, obey SE kinetics, as was found by fitting the curves shown in Figs. 1 and 2. From this fact alone it cannot be concluded that structural relaxation and MDA are related since most monotonically decreasing functions can probably be described by a SE. On the contrary, when the SE parameters describing structural relaxation are compared with those of MDA, a pronounced difference appears. The stretching parameter of relaxation in *a*-Si exhibits only a very weak temperature dependence far removed from that describing MDA and H diffusion in *a*-Si:H.[103] In our opinion this indicates that structural relaxation (as defined in the Introduction) in pure *a*-Si and MDA are distinct processes. This is not to say that defects are unimportant for structural relaxation, rather that the nature of the defects and the defect annealing processes related to structural relaxation (as discussed in Secs. VII and VIII) and MDA are different.

It would be surprising if structural relaxation and MDA were one and the same not only because MDA has been convincingly related to H diffusion but also because structural relaxation is, contrary to the conductivity changes in *a*-Si:H, irreversible (with irreversible we mean that the *a*-Si can only be derelaxed using processes far from thermal equilibrium, see, e.g., Sec. VII). This was further tested by submitting pure *a*-Si to repeated light soaking [1000 W/m^2, Air Mass 1 (AM 1) filtered] and thermal annealing (45 min at 300 °C or 500 °C). Before and after each of these treatments the state of relaxation of the *a*-Si was measured by Raman spectroscopy. No difference could be detected due to the light soaking, which may confirm that structural relaxation and metastable-defect annealing are distinct processes.

E. Structural relaxation in other materials

One of the first questions raised by the suggestion that structural relaxation in *a*-Si is in fact point-defect annihilation is the following: what about relaxation in other solids? A few remarks have already been made regarding structural relaxation in amorphous Ge (*a*-Ge). The similarity between Si and Ge, both in the crystal as well as in the amorphous phase, implies that structural relaxation in *a*-Ge is probably also defect controlled. In this respect it may be recalled that structural relaxation similar to that in *a*-Si has been observed in *a*-Ge by calorimetry,[63,64] Raman scattering,[75] XRD,[76] and EXAFS.[77]

Metallic glasses form an important group of amorphous solids.[154] Here, two types of relaxation have been observed, namely, reversible and irreversible relaxation.[155,156] Reversible relaxation has been associated with chemical short-range ordering which is of course absent in an elemental system such as *a*-Si. Irreversible relaxation can be well described by a free-volume theory and is thought to be mediated by changes in topological short-range order. Free volume is a concept which is defined in a random close packed (RCP) glass but has no meaning in a network glass.[157–159] The difference in bonding between metallic glasses and *a*-Si (i.e., metallic versus covalent)

therefore severely limits the extent to which relaxation in the two materials can be compared.

Computer simulations show that vacancies are stable in a covalent random network but not in a dense random packed model[140] (the potentials used for energy minimization were a Keating potential for the CRN and a Lennard-Jones potential for the RCP model). More recent simulations of irradiation damage in a Lennard-Jones RCP solid show a similar trend.[160] It would not be surprising therefore if the role of point defects and defect annihilation is more pronounced in structural relaxation of *a*-Si than in amorphous metals although it has been recognized that localized structural imperfections probably do play a role in the latter.[161,162]

Finally, we should relate the results and conclusions presented in this paper to structural relaxation in oxide and other covalently bonded network glasses.[150] In these materials, relaxation involves changes in, e.g., viscosity and density. Even though *a*-Si is not a glass,[55] it has been observed to flow plastically even at very low temperatures.[163] More recently, it has been observed that the viscosity of *a*-Si depends on the state of relaxation.[52] In this regard, *a*-Si does behave like a covalently bonded network glass. However, *a*-Si is not a glass[55] because it exhibits a first-order melting transition to metallic liquid Si (*l*-Si) rather than a glass transition.[164,165] In the hypothetical absence of the metallic liquid phase, an extrapolation of the Gibbs free-energy difference between *a*-Si and *c*-Si shows that they are in equilibrium at ≈ 2500 K.[34,64,166] Likewise, Turnbull extrapolated the self-diffusivity in *c*-Si and found for *a*-Si a "virtual" glass temperature of $T_g \approx 1850$ K.[167] This would be the range of temperatures where a semiconducting liquid Si phase might form if *a*-Si were a glass (or if melting to metallic *l*-Si could be avoided).

Typical temperatures T_{relax} for relaxation processes as described in this paper should be scaled to T_g when comparing *a*-Si to normal glasses. It is then seen that structural relaxation in *a*-Si occurs at $T_{relax}/T_g \approx 0.2-0.4$, whereas relaxation in oxide glasses proceeds at a measurable rate only close to T_g.[150] Nevertheless, the fact that *a*-Si is a covalently bonded disordered network in which structural relaxation seems to be dominated by point-defect annihilation suggests that a similar mechanism may be operative in oxide glasses. It would be interesting to compare structural relaxation and radiation damage annealing in glasses with this in mind.

IX. CONCLUSION

In conclusion, we have studied the structure and relaxation phenomena of amorphous Si (*a*-Si), prepared by ion implantation, vacuum evaporation, and laser quenching. Different states of relaxation of *a*-Si, induced either by thermal annealing of as-prepared *a*-Si or by ion bombardment of relaxed *a*-Si, have been characterized using differential scanning calorimetry, Raman spectroscopy, and x-ray diffraction. The heat of crystallization of *a*-Si has been determined to be 13.7 ± 0.3 kJ/mol and the heat of relaxation may amount to an additional 5.3 kJ/mol in as-implanted material. The transient behavior of relaxation has been investigated employing isothermal calorimetry and found to obey bimolecular reaction kinetics. The results suggest that in this material structural relaxation, also known as short-range ordering, is in fact annihilation of point defects and small point-defect clusters, similar to defect removal observed when heavily damaged *c*-Si is heated. This process differs from that which operates when metastable defects in *a*-Si:H are annealed, since in pure *a*-Si the defects are not passivated but are expected to be actually removed from the *a*-Si network. The density of defects in unrelaxed *a*-Si appears to be almost two orders of magnitude higher than expected on the basis of electron-spin-resonance measurements, which would imply that the majority of the defects cannot be detected by electron-spin resonance. Removal of such an amount of defects by mutual annihilation is expected to modify average structural properties such as the average bond-angle distortion.

Note added in proof. It is mentioned in the Introduction and in Sec. VIII C that the density of *a*-Si does not change more than 0.1% upon relaxation. Recent wafer-curvature measurements show that a small ($\leq 0.1\%$) reversible density change exists.[168] Such a density change is not incompatible with the defect processes invoked to explain structural relaxation of *a*-Si.

ACKNOWLEDGMENTS

It is a pleasure to acknowledge J. A. Yater (Cornell University) for preparing the laser-quenched *a*-Si, L. Shapiro and J. Bell (Harvard University), and R. Hettema for assistance with DSC, Michael O. Thompson, J. S. Custer (Cornell University), A. Polman (AT&T), and F. W. Saris (FOM) for discussions, F. Unterwald (AT&T) for the use of his furnace, S. Doorn, J. Derks, R. Koper, and H. Zeijlemaker (FOM) for technical assistance, A. E. White and K. Short (AT&T) for He^+-ion implants, and L. A. Verhoef (FOM) for light soaking. We also wish to thank Ann Witvrouw (Harvard University) for pointing out the relevance of bimolecular reaction kinetics. This work is part of the research program of the Stichting voor Fundamenteel Onderzoek der Materie (FOM) and was made possible by financial support from the Nederlandse Organisatie voor Wetenschappelijk Onderzoek (NWO) and the Stichting voor Technische Wetenschappen (STW). Work at Harvard was supported by the USA National Science Foundation through the Harvard Materials Research Laboratory under Contract No. DMR-86-14003.

*Present address: Université de Montréal, Departement de Physique, Case Postale 6128, succ. "A", Montréal, Quebec, Canada H3C 3J7.

†Present address: Netherlands Energy Research Foundation ECN, P.O. Box 1, 1755 ZG Petten, The Netherlands.

‡Present address: Harrison M. Randall Laboratory of Physics, University of Michigan, Ann Arbor, MI 48109-1120.

[1] D. E. Polk and D. S. Boudreaux, Phys. Rev. Lett. **31**, 92 (1973).

[2] F. Wooten, K. Winer, and D. Weaire, Phys. Rev. Lett. **54**, 1392 (1985).

[3]F. Wooten and D. Weaire, in *Solid State Physics: Advances in Research Applications,* edited by D. Turnbull and H. Ehrenreich (Academic, New York, 1987), Vol. 40, pp. 2–42.
[4]R. Car and M. Parrinello, Phys. Rev. Lett. **60**, 204 (1988).
[5]T. Uda, Solid State Commun. **64**, 837 (1987).
[6]R. Biswas, G. S. Crest, and C. M. Soukoulis, Phys. Rev. B **36**, 7473 (1987).
[7]W. E. Spear and P. G. LeComber, Solid State Commun. **17**, 1193 (1975).
[8]W. E. Spear and P. G. LeComber, Philos. Mag. **33**, 935 (1976).
[9]D. E. Carlson and C. R. Wronksi, Appl. Phys. Lett. **28**, 671 (1976).
[10]P. A. Thomas, M. H. Brodsky, D. Kaplan, and D. Lepine, Phys. Rev. B **18**, 3059 (1978).
[11]W. G. Spitzer, G. K. Huber, and T. A. Kennedy, Nucl. Instrum. Methods **209/210**, 309 (1983).
[12]R. A. Street, Adv. Phys. **30**, 593 (1981).
[13]J. E. Frederickson, C. N. Waddell, W. G. Spitzer, and G. K. Hubler, Appl. Phys. Lett. **40**, 172 (1982).
[14]G. K. Hubler, E. P. Donovan, K. W. Wang, and W. G. Spitzer, Soc. Photo-Opt. Instrum. Eng. **530**, 222 (1985).
[15]E. P. Donovan, G. K. Hubler, and C. N. Waddell, Nucl. Instrum. Methods B **19/20**, 590 (1987).
[16]R. H. Klazes, M. H. L. M. van den Broek, J. Bezemer, and S. Radelaar, Philos. Mag. B **45**, 377 (1982).
[17]G. Müller and S. Kalbitzer, Non-Cryst. Solids 278 (1977).
[18]D. L. Staebler and C. R. Wronski, Appl. Phys. Lett. **31**, 292 (1977).
[19]R. Tsu, J. G. Hernandez, J. Doehler, and S. R. Ovshinsky, Solid State Commun. **46**, 79 (1983).
[20]J. S. Lannin, L. J. Pilione, S. T. Kshirsagar, R. Messier, and R. C. Ross, Phys. Rev. B **26**, 3506 (1982).
[21]W. C. Sinke, T. Warabisako, M. Miyao, T. Tokuyama, S. Roorda, and F. W. Saris, J. Non-Cryst. Solids **99**, 308 (1988).
[22]S. Roorda, S. Doorn, W. C. Sinke, P. M. L. O. Scholte, and E. van Loenen, Phys. Rev. Lett. **62**, 1880 (1989).
[23]E. P. Donovan, F. Spaepen, J. M. Poate, and D. C. Jacobson, Appl. Phys. Lett. **55**, 1516 (1989).
[24]S. C. Moss and J. F. Graczyk, Phys. Rev. Lett. **23**, 1167 (1969).
[25]S. C. Moss and J. F. Graczyk, in *Proceedings of the 10th International Conference on the Physics of Semiconductors,* edited by S. Keller (Cambridge, Massachusetts, 1970), p. 658.
[26]R. Mosseri, C. Sella, and J. Dixmier, Phys. Status Solidi A **52**, 475 (1979).
[27]S. Roorda, W. C. Sinke, J. M. Poate, D. C. Jacobson, P. Fuoss, S. Dierker, B. S. Dennis, and F. Spaepen, in *Beam-Solid Interactions: Physical Phenomena,* edited by P. Børgesen, MRS Symposia Proceedings No. 157 (Materials Research Society, Pittsburgh, 1990), p. 683.
[28]A. Di Cicco, A. Bianconi, C. Coluzza, P. Rudolf, P. Lagarde, A. M. Flank, and A. Marcelli, J. Non-Cryst. Solids **116**, 27 (1990).
[29]J. C. Bean and J. M. Poate, Appl. Phys. Lett. **36**, 59 (1980).
[30]M. H. Brodsky, D. Kaplan, and J. F. Ziegler, Appl. Phys. Lett. **21**, 305 (1972).
[31]J. Fortner and J. S. Lannin, Phys. Rev. B **39**, 5527 (1989).
[32]K. Tanaka and A. Matsuda, Mater. Sci. Rep. **2**, 139 (1987).
[33]J. S. Custer, M. O. Thompson, D. C. Jacobson, J. M. Poate, S. Roorda, W. C. Sinke, and F. Spaepen, Appl. Phys. Lett. (to be published); in *Beam-Solid Interactions: Physical Phenomena* (Ref. 27), p. 689.
[34]W. C. Sinke, S. Roorda, and F. W. Saris, J. Mater. Res. **3**, 1201 (1988).
[35]J. S. Lannin, Phys. Today **41** (7), 28 (1988); J. Non-Cryst. Solids **97/98**, 39 (1987).
[36]S. Roorda, thesis, University of Utrecht, 1990.
[37]S. Roorda, J. M. Poate, D. C. Jacobson, D. J. Eaglesham, B. S. Dennis, S. Dierker, W. C. Sinke, and F. Spaepen, Solid State Commun. **75**, 197 (1990).
[38]S. Roorda, W. C. Sinke, J. M. Poate, D. C. Jacobson, S. Dierker, and B. S. Dennis, Appl. Phys. Lett. **56**, 2097 (1990).
[39]S. Roorda, W. C. Sinke, J. M. Poate, D. C. Jacobson, S. Dierker, B. S. Dennis, D. J. Eaglesham, and F. Spaepen, in *Beam-Solid Interactions: Physical Phenomena* (Ref. 27), p. 709.
[40]G. A. Norton, R. E. Daniel, R. L. Loger, and J. B. Schroeder, Nucl. Instrum. Methods B **37/38**, 403 (1989).
[41]A. Polman *et al.*, Nucl. Instrum. Methods B **37/38**, 935 (1989).
[42]L. R. Doolittle, Nucl. Instrum. Methods B **9**, 344 (1985); **15**, 227 (1986).
[43]D. C. Santry and R. D. Werner, Nucl. Instrum. Methods **159**, 523 (1979); **178**, 523 (1980).
[44]D. C. Santry and R. D. Werner, Nucl. Instrum. Methods **188**, 211 (1981).
[45]The original RBS measurements (Ref. 27) were in error and overestimated the thickness of the *a*-Si layers. Therefore a small difference occurs between the values for the molar heat release due to relaxation and crystallization presented in this paper and in Ref. 27.
[46]S. Saitoh, T. Sugii, H. Ishiwara, and S. Furukawa, Jpn. J. Appl. Phys. **20**, L130 (1981).
[47]J. A. Yater and M. O. Thompson, Phys. Rev. Lett. **63**, 2088 (1989).
[48]J. F. Ziegler, J. P. Biersack, and U. Littmark, *The Stopping and Range of Ions in Solids* (Pergamon, New York, 1985).
[49]The TRIM version 4.4 (1988) was used (Refs. 48 and 50), vacancy production may vary by a factor of 2 between different versions.
[50]J. P. Biersack and L. J. Haggmark, Nucl. Instrum. Methods **174**, 257 (1980).
[51]R. Tsu, J. G. Hernandez, and F. H. Pollak, Solid State Commun. **54**, 447 (1985).
[52]A. Witvrouw and F. Spaepen, in *Kinetics of Phase Transformations,* edited by M. O. Thompson, M. J. Aziz, and G. B. Stephenson, MRS Symposia Proceedings No. 205 (Materials Research Society, Pittsburgh, in press).
[53]V. Vand, Proc. Phys. Soc. London Sect. A **55**, 222 (1943); W. Primak, Phys. Rev. **100**, 1677 (1955).
[54]M. R. J. Gibbs, J. E. Evetts, and J. A. Leake, J. Mater. Sci. **18**, 278 (1983).
[55]J. M. Poate, in *Amorphous Silicon and Related Materials,* edited by H. Fritzsche (World Scientific, Singapore, 1989), Vol. 1A, p. 149.
[56]G. L. Olson and J. A. Roth, Mater. Sci. Rep. **3**, 1 (1988).
[57]F. Spaepen and C. V. Thompson, Appl. Surf. Sci. **38**, 1 (1989).
[58]T. Papa, F. Scudieri, M. Marinelli, U. Zammit, and G. Cembali, J. Phys. (Paris) **44**, C5-73 (1983).
[59]D. G. Cahill, H. E. Fischer, T. Klitsner, E. T. Schwartz, and R. O. Pohl, J. Vac. Sci. Technol. A **7**, 1259 (1989).
[60]H. J. Goldsmid and G. L. Paul, Thin Solid Films **103**, L47 (1983).
[61]P. Nath and K. L. Copra, Phys. Rev. B **10**, 3412 (1974).
[62]P. B. Allen and J. L. Feldman, Phys. Rev. Lett. **62**, 645 (1989).
[63]H. S. Chen and D. Turnbull, J. Appl. Phys. **40**, 4214 (1969).
[64]E. P. Donovan, F. Spaepen, D. Turnbull, J. M. Poate, and D. C. Jacobson, J. Appl. Phys. **57**, 1795 (1985).

[65]J. C. C. Fan and C. H. Anderson, Jr., J. Appl. Phys. **52**, 4003 (1981).
[66]L. de Wit, S. Roorda, W. C. Sinke, F. W. Saris, A. J. M. Berntsen, and W. F. van der Weg, in *Kinetics of Phase Transformations* (Ref. 52).
[67]R. Shuke and R. W. Gammon, Phys. Rev. Lett. **25**, 222 (1970).
[68]D. Beeman, R. Tsu, and M. F. Thorpe, Phys. Rev. B **32**, 874 (1985).
[69]R. Tsu, Solar Cells **21**, 19 (1987).
[70]T. Ishidate, K. Inoue, T. Tsuji, and S. Minomura, Solid State Commun. **42**, 197 (1982).
[71]T. Saito, T. Karasawa, and I. Ohdomari, J. Non-Cryst. Solids **50**, 271 (1982).
[72]P. N. Keating, Phys. Rev. **145**, 637 (1966).
[73]R. Alben, D. Weaire, J. E. Smith, Jr., and M. H. Brodsky, Phys. Rev. B **11**, 2271 (1975).
[74]C. K. Wong and G. Lucovsky, in MRS Symposia Proceedings No. 70, edited by D. Adler, Y. Hamakawa, and A. Madan (Materials Research Society, Pittsburgh, 1986), p. 77.
[75]J. Fortner and J. S. Lannin, Phys. Rev. B **37**, 10 154 (1988).
[76]R. J. Temkin, W. Paul, and G. A. N. Connell, Adv. Phys. **22**, 581 (1973).
[77]M. A. Paesler, D. E. Sayers, R. Tsu, and J. G. Hernandez, Phys. Rev. B **28**, 4550 (1983).
[78]See, for instance, M. H. Brodsky, R. S. Title, K. Weiser, and G. D. Pettit, Phys. Rev. B **1**, 2632 (1970), and references cited therein.
[79]R. Tsu, R. T. Hodgson, T. Y. Tan, and J. E. Baglin, Phys. Rev. Lett. **42**, 1356 (1979).
[80]A. G. Cullis, H. C. Webber, N. G. Chew, J. M. Poate, and P. Baeri, Phys. Rev. Lett. **49**, 219 (1982).
[81]A. G. Cullis, in *Energy Beam-Solid Interactions and Transient Thermal Processing,* edited by V. T. Nguyen and A. G. Cullis (Les Editions de Physique, Les Ulis Cedex, 1985), pp. 45–55.
[82]J. J. P. Bruines, Thesis Eindhoven Technical University, The Netherlands, 1988.
[83]R. Tsu, J. G. Hernandez, and F. H. Pollak, J. Non-Cryst. Solids **66**, 109 (1984).
[84]N. Maley, J. S. Lannin, and A. G. Cullis, Phys. Rev. Lett. **53**, 1571 (1984).
[85]J. S. Custer, M. O. Thompson, and P. H. Bucksbaum, Appl. Phys. Lett. **53**, 1402 (1988).
[86]M. O. Thompson, G. J. Galvin, J. W. Mayer, P. S. Peercy, J. M. Poate, D. C. Jacobson, A. G. Cullis, and N. G. Chew, Phys. Rev. Lett. **52**, 2360 (1984).
[87]W. C. Sinke, T. Warabisako, M. Miyao, T. Tokuyama, S. Roorda, and F. W. Saris, in *Photon, Beam and Plasma Enhanced Processing,* edited by A. Golanski, V. T. Nguyen, and E. F. Krimmel (Les Editions de Physique, Les Ulis Cedex, 1987), pp. 279–284.
[88]M. O. Thompson, S. Roorda, M. J. Aziz, and P. C. Peercy (unpublished).
[89]S. Roorda and W. C. Sinke, in *Kinetics of Phase Transformations* (Ref. 52).
[90]A. Mesli, J. C. Muller, and P. Siffert, J. Phys. (Paris) **44**, C5-281 (1983).
[91]R. T. Young, R. F. Wood, W. H. Cristie, and G. E. Jellison, Jr., Appl. Phys. Lett. **39**, 313 (1981).
[92]J. L. Benton, C. J. Doherty, S. D. Ferris, D. L. Flamm, L. C. Kimerling, and H. J. Leamy, Appl. Phys. Lett. **36**, 670 (1980).
[93]P. M. Mooney, R. T. Young, J. Karins, Y. H. Lee, and J. W. Corbett, Phys. Status Solidi A **48**, K31 (1978).
[94]P. L. Lui, R. Yen, N. Bloembergen, and R. T. Hodgson, Appl. Phys. Lett. **34**, 864 (1979).
[95]W. E. Spear, in *5th International Conference on Amorphous and Liquid Semiconductors,* edited by J. Stuke and W. Brenig (Taylor & Francis, London, 1974), p. 1.
[96]W. Beyer, J. Stuke, and H. Wagner, Phys. Status Solidi **30**, 231 (1975).
[97]G. Müller, S. Kalbitzer, W. E. Spear, and P. G. Le Comber, in *Proceedings of the 7th International Conference on Amorphous and Liquid Semiconductors,* edited by W. E. Spear (CICL, University of Edinburgh, 1977), p. 442.
[98]R. Street, D. Biegelsen, and J. Stuke, Philos. Mag. B **40**, 451 (1979).
[99]G. Müller and P. G. Le Comber, Philos. Mag. B **43**, 419 (1981).
[100]C. E. Michelson, J. D. Cohen, and J. P. Harbison, in *Amorphous Silicon Semiconductors—Pure and Hydrogenated,* edited by A. Madan, M. Thompson, D. Adler, and Y. Hamakawa, MRS Symposia Proceedings Vol. 95 (Materials Research Society, Pittsburgh, 1987), p. 71.
[101]D. L. Staebler and C. R. Wronski, J. Appl. Phys. **51**, 3262 (1980).
[102]J. Kakalios, R. A. Street, and W. B. Jackson, Phys. Rev. Lett. **59**, 1037 (1987).
[103]R. A. Street, in *Amorphous Silicon Semiconductors—Pure and Hydrogenated* (Ref. 100), p. 13.
[104]W. K. Chu, J. W. Mayer, and M. A. Nicolet, *Backscattering Spectrometry* (Academic, New York, 1978).
[105]L. C. Feldman, J. W. Mayer, and S. T. Picraux, *Materials Analysis by Ion Channeling* (Academic, New York, 1982).
[106]Y. Shih, J. Washburn, E. R. Weber, and R. Gronsky, in *Ion Beam Processes in Advanced Electronic Material & Device Technology,* edited by B. R. Appleton, F. H. Eisen, and T. W. Sigmun, MRS Symposia Proceedings Vol. 45 (Materials Research Society, Pittsburgh, 1985), p. 65.
[107]J. R. Dennis and E. B. Hale, J. Appl. Phys. **49**, 1119 (1978).
[108]J. Washburn, C. S. Murty, D. Sadana, P. Byrne, R. Gronsky, N. Cheung, and R. Kilaas, Nucl. Instrum. Methods **209/210**, 345 (1983).
[109]A. Battaglia, F. Priolo, E. Rimini, and G. Ferla, Appl. Phys. Lett. **56**, 2623 (1990).
[110]See, for example, *Radiation Effects in Semiconductors,* edited by J. W. Corbett and G. D. Watkins (Gordon and Breach, New York, 1971).
[111]M. O. Ruault, J. Chaumont, and H. Bernas, Nucl. Instrum. Methods **209/210**, 351 (1983).
[112]M. O. Ruault, J. Chaumont, J. M. Penisson, and A. Bourret, Philos. Mag. A **50**, 667 (1984).
[113]J. C. Bourgoin, J. F. Morhange, and R. Beserman, Radiat. Eff. **22**, 205 (1974).
[114]M. Balkanski, J. F. Morhange, and G. Kanellis, J. Raman Spectrosc. **10**, 240 (1981).
[115]A. C. deWilton, M. Simard-Normandind, and P. T. T. Wong, J. Electrochem. Soc. **133**, 989 (1986).
[116]W. C. Sinke, T. Warabisako, M. Miyao, T. Tokuyama, and S. Roorda, Appl. Surf. Sci. **36**, 460 (1989).
[117]J. E. Smith, Jr., M. H. Brodsky, B. L. Crowder, and M. I. Nathan, J. Non-Cryst. Solids **8-10**, 179 (1972).
[118]T. Shimada, Y. Katayama, K. Nakagawa, H. Matsubara, M. Migitaki, and E. Maruyama, J. Non-Cryst. Solids **59/60**, 783 (1983).
[119]K. W. Wang, W. G. Spitzer, G. K. Hubler, and D. K. Sadana, J. Appl. Phys. **58**, 4553 (1985).
[120]K. S. Jones, S. Prussin, and E. R. Weber, Appl. Phys. A **45**, 1 (1988).
[121]D. A. Thompson, A. Golanski, H. K. Haugen, L. M. Howe,

and J. A. Davies, Radiat. Eff. **50**, 125 (1980).

[122]P. H. Fang, Phys. Lett. **27A**, 697 (1968); **30A**, 219 (1969); M. Hirata, M. Hirata, H. Saito, and J. H. Crawford, in *Lattice Defects in Semiconductors,* edited by R. R. Hasiguti (University of Tokyo Press, Tokyo, 1968), p. 159.

[123]J. W. Mayer, in *Radiation Effects in Semiconductors,* edited by J. W. Corbett and G. D. Watkins (Gordon and Breach, London, 1971), p. 367.

[124]K. A. Jackson, J. Mater. Res. **3**, 1218 (1988).

[125]S. Dannefaer, P. Mascher, and D. Kerr, Phys. Rev. Lett. **56**, 2195 (1986).

[126]A. Polman, D. C. Jacobson, S. Coffa, J. M. Poate, S. Roorda, and W. C. Sinke, Appl. Phys. Lett. **57**, 1230 (1990).

[127]S. Coffa, J. M. Poate, D. C. Jacobson, and A. Polman, Appl. Phys. Lett. (to be published).

[128]S. Coffa, D. C. Jacobson, J. M. Poate, W. Frank, and W. Gustin (unpublished).

[129]J. M. Poate, D. C. Jacobson, J. S. Williams, R. G. Elliman, and D. O. Boerma, Nucl. Instrum. Methods B **19/20**, 480 (1987).

[130]L. Calcagno, S. U. Campisano, and S. Coffa, J. Appl. Phys. **66**, 1874 (1989).

[131]E. Nygren, B. Park, L. M. Goldman, and F. Spaepen, Appl. Phys. Lett. **56**, 2094 (1990).

[132]J. M. Poate, D. C. Jacobson, F. Priolo, and M. O. Thompson, in *Processing and Characterization of Materials Using Ion Beams,* edited by L. E. Rehn, J. Greene, and F. A. Smidt, MRS Symposia Proceedings Vol. 128 (Materials Research Society, Pittsburgh, 1989), p. 533.

[133]H. S. Chen, L. C. Kimerling, J. M. Poate, and W. L. Brown, Appl. Phys. Lett. **32**, 461 (1978).

[134]K. F. Heidemann, M. Grüner, and E. te Kaat, Radiat. Eff. **82**, 103 (1984).

[135]P. Hautojärvi, P. Huttunen, J. Mäkinen, E. Punka, and A. Vehanen, in *Defects in Electronic Materials,* edited by M. Stavola, S. J. Pearton, and J. Davies, MRS Symposia Proceedings Vol. 104 (Materials Research Society, Pittsburgh, 1988), p. 105.

[136]D. Adler, Phys. Rev. Lett. **41**, 1755 (1978).

[137]*Point Defects in Solids,* edited by J. H. Crawford and L. M. Slifkin (Plenum, New York, 1975), Vol. 2, p. 4.

[138]S. Y. Tong, H. Huang, C. M. Wei, W. E. Packard, F. K. Men, G. Glander, and M. B. Webb, J. Vac. Sci. Technol. A **6**, 615 (1988).

[139]A. Antonelli and J. Bernholc, in *Impurities, Defects and Diffusion in Semiconductors: Bulk and Layered Structures,* edited by D. J. Wolford, J. Bernholc and E. E. Haller, MRS Symposia Proceedings Vol. 163 (Materials Research Society, Pittsburgh, 1990), p. 523.

[140]C. H. Bennett, P. Chaudhari, V. Moruzzi, and P. Steinhardt, Philos. Mag. A **40**, 485 (1979).

[141]F. L. Vook, Phys. Rev. **125**, 855 (1962).

[142]For recent reviews, see *Advances in Disordered Semiconductors,* edited by H. Fritzsche (World Scientific, Singapore, 1989), Vols. 1A and 1B.

[143]H. Dersch, J. Stuke, and J. Beichler, Appl. Phys. Lett. **38**, 456 (1981).

[144]S. T. Pantelides, Phys. Rev. Lett. **57**, 2979 (1986).

[145]S. T. Pantelides, Phys. Rev. Lett. **58**, 1344 (1987).

[146]Z. E. Smith and S. Wagner, Phys. Rev. B **32**, 5510 (1985).

[147]D. Redfield and R. H. Bube, Appl. Phys. Lett. **54**, 1037 (1989).

[148]G. Williams and D. C. Watts, Trans. Faraday Society **66**, 80 (1970).

[149]R. Kohlrausch, Poggendorff's Annal. **12** (3), 353 (1847).

[150]G. W. Scherer, *Relaxation in Glass and Composites* (Wiley, New York, 1986).

[151]M. Pruppers, thesis, Utrecht University, 1988, p. 124.

[152]W. B. Jackson, Appl. Surf. Sci. **39**, 273 (1989).

[153]W. B. Jackson, J. M. Marshall, and M. D. Moyer, Phys. Rev. B **39**, 1164 (1989).

[154]See, for example, *Metastable Alloys: Preparation and Properties,* Proceedings of the European Materials Research Society Symposium on Preparation and Properties of Metastable Alloys, edited by K. Samwer, M. von Allmen, J. Bøttiger, and B. Stritzker (North-Holland, Amsterdam, 1989).

[155]T. Egami, Ann. N.Y. Acad. Sci. **371**, 238 (1981).

[156]J. O. Ström-Olsen, R. Brüning, Z. Altounian, and D. H. Ryan, J. Less-Common Metals **145**, 327 (1988).

[157]D. Turnbull and M. H. Cohen, J. Chem. Phys. **34**, 120 (1961).

[158]D. Turnbull and M. H. Cohen, J. Chem. Phys. **52**, 3038 (1970).

[159]R. Zallen, *The Physics of Amorphous Solids* (Wiley-Interscience, New York, 1983).

[160]J. Laakkonen and R. M. Nieminen, Phys. Rev. B **41**, 3978 (1990).

[161]F. Spaepen, J. Non-Cryst. Solids **31**, 207 (1978).

[162]D. Srolovitz, T. Egami, and V. Vitek, Phys. Rev. B **24**, 6936 (1981).

[163]C. A. Volkert, Mater. Res. Soc. Symp. Proc. **157**, 635 (1990).

[164]F. Spaepen and D. Turnbull, in *Laser-Solids Interactions and Laser Processing,* edited by S. D. Ferris, H. J. Leamy, and J. M. Poate, AIP Conf. Proc. No. 50 (AIP, New York, 1979), p. 73.

[165]B. G. Bagley and H. S. Chen, in *Laser-Solids Interactions and Laser Processing* (Ref. 164), p. 97.

[166]S. Roorda and W. C. Sinke, Appl. Surf. Sci. **36**, 588 (1989).

[167]D. Turnbull, in *Metastable Materials Formation by Ion Implantation,* edited by S. T. Picraux and W. J. Choyke (Elsevier Science, New York, 1982), p. 103.

[168]C. A. Volkert (unpublished).

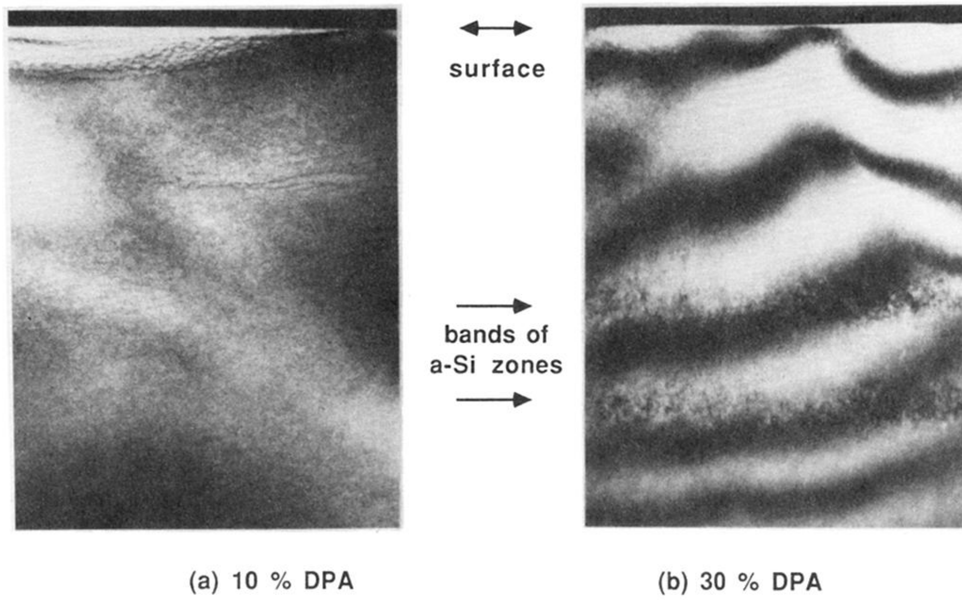

FIG. 12. TEM micrographs of (a) 0.1 DPA and (b) 0.3 DPA He^{+}-ion bombarded *c*-Si, before DSC measurements. Arrows indicate position of the surface and bands of defects.